

A conserved morphogenetic mechanism for epidermal ensheathment of nociceptive sensory neurites

Nan Jiang¹, Jeffrey P. Rasmussen^{2†}, Joshua A. Clanton², Marci F. Rosenberg², Kory P. Luedke¹, Mark R. Cronan⁵, Ed Parker³, Hyeon-Jin Kim⁴, Joshua C. Vaughan⁴, Alvaro Sagasti², Jay Z. Parrish^{1*}

¹Department of Biology, University of Washington, Seattle, WA 98195

²Department of Molecular, Cell, and Developmental Biology, University of California Los Angeles, Los Angeles, CA 90095

³Department of Ophthalmology, University of Washington, Seattle, WA 98195

⁴Department of Chemistry and Department of Department of Physiology and Biophysics, University of Washington, Seattle, WA 98195

⁵Department of Molecular Genetics and Microbiology, Duke University, Durham, NC 27710

[†]Current address: Department of Biology, University of Washington, Seattle, WA 98195

*Correspondence should be addressed to J.Z.P (jzp2@uw.edu)

Abstract

Interactions between epithelial cells and neurons influence a range of sensory modalities including taste, touch, and smell. Vertebrate and invertebrate keratinocytes/keratinocyte-like epidermal cells ensheath peripheral arbors of somatosensory neurons, including nociceptors, yet the developmental origins and functional roles of this ensheathment are largely unknown. Here, we describe an evolutionarily conserved morphogenetic mechanism for epidermal ensheathment of somatosensory neurites. We found that somatosensory neurons in *Drosophila* and zebrafish induce formation of epidermal sheaths, which wrap neurites of different types of neurons to different extents. Neurites induce formation of plasma membrane phosphatidylinositol 4,5-bisphosphate microdomains at nascent sheaths, followed by a filamentous actin network, and recruitment of junctional proteins that likely form autotypic junctions to seal sheaths. Finally, blocking epidermal sheath formation destabilized dendrite branches and reduced nociceptive sensitivity in *Drosophila*. Epidermal somatosensory neurite ensheathment is thus a deeply conserved cellular process that contributes to the morphogenesis and function of nociceptive sensory neurons.

Introduction

The innervation patterns of cutaneous receptors determine our responses to external stimuli. Many types of cutaneous receptors form specialized terminal structures with epithelial cells that contribute to somatosensation (Owens and Lumpkin 2014; Zimmerman, Bai, and Ginty 2014). For example, some low threshold mechanoreceptor afferents form synapse-like contacts with Merkel cells (Mihara et al. 1979), which directly respond to mechanical stress and tune gentle touch responses (Maksimovic et al. 2014; Woo et al. 2014). Similarly, afferent interactions with radially packed Schwann cell-derived lamellar cells in Pacinian corpuscles facilitate high frequency sensitivity (Loewenstein and Skalak 1966). By contrast, although various types of free nerve endings, including nociceptive C-fibers, course over and insert into keratinocytes, much less is known about the anatomy of keratinocyte-sensory neuron coupling, or the mechanisms by which keratinocytes modulate sensory neuron structure and function. Recent findings that keratinocytes express sensory channels (Peier et al. 2002; Bidaux et al. 2015; Y. Chen et al. 2016), respond to sensory stimuli (Koizumi et al. 2004; Xu et al. 2006; Moehring et al. 2018), release compounds that modulate sensory neuron function (Woolf et al. 1997; Koizumi et al. 2004; Moehring et al. 2018), and can drive sensory neuron firing (Baumbauer et al. 2015; Pang et al. 2015), underscore the importance of understanding the coupling of keratinocytes to sensory neurons.

Anatomical studies have demonstrated that peripheral arbors of some mammalian somatosensory neurons insert into keratinocytes, not just intercalate between them (Munger 1965; Cauna 1973). Several factors have hindered characterization of sensory neuron-keratinocyte interactions in mammalian systems,

including region-specific differences in sensory neuron-epidermis interactions (Kawakami, Ishihara, and Mihara 2001; Liu et al. 2014), a still-growing repertoire of neuronal cell types that innervate the epidermis (Usoskin et al. 2015; Nguyen et al. 2017), and a shortage of markers that label discrete populations of sensory neurons. Peripheral arbors of somatosensory neurons are likewise inserted into keratinocytes or keratinocyte-like epidermal cells in invertebrate and non-mammalian vertebrate model systems, making these promising settings for characterizing epithelial cell-neurite interactions. Notably, portions of *Drosophila melanogaster* larval nociceptive class IV dendrite arborization (da) neuron dendrites and *Danio rerio* (zebrafish) larval trigeminal and Rohon-Beard (RB) sensory axons become ensheathed by epidermal cells (Han et al. 2012; Kim et al. 2012; O'Brien et al. 2012), and studies in these systems have provided insight into the structure and possible function of this epidermal ensheathment of free nerve endings.

Drosophila and zebrafish epidermal cells wrap sensory neurites by extending membranes around the entire circumference of the sensory neurite. The wrapping epidermal membranes are tightly apposed to one another and the ensheathed neurites, embedding them inside a mesaxon-like structure (Whitewar and Moate 1998; Han et al. 2012; Kim et al. 2012; O'Brien et al. 2012). A similar structure has been documented for ensheathed somatosensory neurites in *Caenorhabditis elegans* and humans (Cauna 1973; Chalfie and Sulston 1981), suggesting that ensheathment by epidermal cells is a conserved feature of sensory endings. The most extensive ultrastructural analysis of these structures suggests that the sensory neurites can be continuously ensheathed over extended lengths of the arbor, stretching several micrometers or more (O'Brien et

al. 2012). Structurally, the interaction between keratinocytes and somatosensory neurites is reminiscent of ensheathment of peripheral axons by nonmyelinating Schwann cells in Remak bundles, suggesting that keratinocyte ensheathment may likewise regulate sensory neuron structure (S. Chen et al. 2003) and function (Orita et al. 2013; Faroni et al. 2014).

Although the extent and distribution of sensory neurite-epidermal ensheathment have not been systematically analyzed, many of the documented instances involve highly branched mechanosensory and/or nociceptive neurons. In *Drosophila*, epidermal ensheathment has been linked to control of branching morphogenesis in two ways. First, nociceptive class IV dendrite arborization (c4da) neurons are largely restricted to a two-dimensional plane along the basal surface of epidermal cells to potentiate contact-dependent repulsion and hence tiling (Han et al. 2012; Kim et al. 2012). However, portions of c4da neurons are apically shifted and ensheathed inside the epidermis, allowing for dendrites of other da neurons to innervate the unoccupied basal space and hence “share” the territory (Tenenbaum et al. 2017). Second, epidermal ensheathment appears to regulate dendrite branching activity, as mutation of the microRNA *bantam*, which regulates dendrite-epidermis interactions (Jiang et al. 2014), or knockdown of *coracle* (*cora*), which encodes a band 4.1-related protein required for sheath formation (Tenenbaum et al. 2017), each increase dendrite branching. Although these studies provide the first signs that epidermal ensheathment plays key roles in somatosensory neuron development, the cellular basis and functional consequences of this sensory neuron-epidermis coupling remain to be determined.

Here, we characterized the cellular events involved in formation of epidermal ensheathment of somatosensory neurites in *Drosophila* and zebrafish. First, we identified a series of reporters that accumulate at epidermal sites of somatosensory dendrite ensheathment in *Drosophila*, demonstrating that sheaths form at specialized membrane domains and providing markers for *in vivo* tracking of the sheaths. Remarkably, epidermal sheaths are labeled by similar markers in zebrafish, suggestive of a conserved molecular machinery for ensheathment. Using these reporters, we found that epidermal sheaths in *Drosophila* and zebrafish wrap different types of neurons to different extents and that somatosensory neurons are required for formation and maintenance of epidermal sheaths. Finally, we found that blocking epidermal sheath formation led to exuberant dendrite branching and branch turnover, as well as reduced nociceptive sensitivity in *Drosophila*. Altogether, these studies demonstrate that epidermal ensheathment of somatosensory neurons by keratinocytes/keratinocyte-like cells is a deeply conserved cellular process that plays key roles in the morphogenesis and function of nociceptive sensory neurons.

Results

PIP2 in epithelial cells is enriched at sites of *Drosophila* dendrite ensheathment

Recent studies demonstrate that large portions of *Drosophila* c4da dendrite arbors are ensheathed by the epidermis (Tenenbaum et al. 2017; Jiang et al. 2018). To gain a high resolution view of this ensheathment over extended length scales we subjected *Drosophila* third instar larvae to serial block-face scanning electron microscopy (SBF-SEM) (Denk and Horstmann 2004). Consistent with prior TEM studies which provided a

snapshot of these sheath structures (Han et al. 2012; Kim et al. 2012; Jiang et al. 2014), in individual sections we observed dendrites embedded inside epithelial cells and connected to the basal epithelial surface by thin, tubular invaginations formed by close apposition of epidermal membranes (Figure 1A). To determine if c4da dendrites were continuously ensheathed in these mesaxon-like structures, we followed individual dendrites from the site of insertion into the epidermis through EM volumes of abdominal segments cut in 60 nm sections along the apical-basal axis. We found that dendrites were embedded in epithelial cells over extended length scales (often several microns or more), that dendrites were continuously embedded in these mesaxon-like structures with elongated tubular invaginations, and that the epidermal membranes comprising the walls of these tubular invaginations were tightly juxtaposed and electron-dense along their entire length (Figure 1B, 1C). Each of these structural elements was previously described for the ensheathment of peripheral axons by keratinocytes in zebrafish (O'Brien et al. 2012), suggesting that the mechanism of epidermal somatosensory neuron ensheathment may be conserved between invertebrates and vertebrates.

We hypothesized that formation of dendrite sheaths likely involves recruitment of factors that create specialized membrane domains. To identify epithelial membrane-associated markers that preferentially localize to sites of dendrite ensheathment, we used the Gal4-UAS system to selectively express GFP-tagged markers in the epidermis of *Drosophila* larvae also expressing the c4da-specific marker *ppk-CD4-tdTomato* and assayed for GFP enrichment at sites of dendrite-epidermis apposition. Whereas the single-pass transmembrane marker CD4-GFP broadly labeled epithelial membranes and showed no obvious enrichment at sites of dendrite contact (Figure 1D, 1E), our

screen of ~90 GFP-tagged membrane- and cytoskeleton-associated proteins yielded several markers that were enriched in basal domains of epithelial cells adjacent to c4da dendrites (Figure 1 – figure supplement 1A, Table S1).

First, we screened a collection of membrane markers to determine whether ensheathment occurs at specialized membrane domains. Among these markers, the phosphatidylinositol 4,5-bisphosphate (PIP₂) probe PLC^δ-PH-GFP (Várnai and Balla 1998; Verstreken et al. 2009) exhibited the most extensive enrichment at sites of epidermal dendrite ensheathment. In epithelial cells of third instar larvae, PLC^δ-PH-GFP accumulated at epithelial cell-cell junctions, punctate patches, and elongated filamentous membrane microdomains adjacent to c4da dendrites (Figure 1F-1K). These PLC^δ-PH-GFP-positive membrane microdomains were also labeled by antibodies to the *Drosophila* 4.1 protein cora (Figure 1 – figure supplement 1B), a previously described marker of epidermal dendrite sheaths (Kim et al. 2012; Tenenbaum et al. 2017), demonstrating that these PLC^δ-PH-GFP-positive microdomains correspond to epidermal dendrite sheaths. In addition to labeling epidermal sheaths, anti-cora immunostaining labels glial sheaths, which wrap axons, cell bodies and proximal dendrites segments of sensory neurons, however, epidermal PLC^δ-PH-GFP was not enriched at these sites of glial ensheathment. PLC^δ-PH-GFP-positive domains often appeared wider than c4da dendrites (Figure 1H-1I), suggesting that PLC^δ-PH-GFP labels the entire sheath structure, including the convoluted tubular extensions to the basal surface of the epidermis.

Since many of the sheath structures are smaller than the axial resolution of a standard confocal microscope, we used expansion microscopy (ExM) to gain a 3-

dimensional view of epidermal PLC^δ-PH-GFP localization adjacent to c4da dendrites (Jiang et al. 2018). We found that PLC^δ-PH-GFP labeled epidermal structures that extend from the most apical extent of dendrite insertion to the basal surface of individual epithelial cells (Figure 1J-1K), suggesting that PLC^δ-PH-GFP indeed labels the entire sheath structure. PLC^δ-PH-GFP was locally depleted at branch points (Figure 1J, white arrows; Figure 1 – figure supplement 1D), consistent with prior observations that dendrite branch points are less extensively ensheathed than dendrite shafts (Tenenbaum et al. 2017). Point mutations in the PH domain of PLC^δ-PH-GFP that abrogate PIP2 binding (Várnai and Balla 1998; Verstreken et al. 2009) prevented accumulation of PLC^δ-PH-GFP at sites of ensheathment (Figure 1 – figure supplement 1C), and we found similar patterns of accumulation at sheaths by other PIP2-binding proteins, including OSH2-PH-GFP (Figure 1 – figure supplement 1E), which binds phosphatidylinositol 4-phosphate and PIP2 with similar affinities (Hardie et al. 2015). Together, these observations demonstrate that epithelial sites of dendrite ensheathment are enriched in PIP2.

PIP2 is a negatively charged phospholipid that recruits a variety of proteins to the plasma membrane to regulate vesicular trafficking and actin remodeling (De Craene et al. 2017), and epithelial cells in *Drosophila* and zebrafish phagocytose peripheral arbors of sensory neurons after injury and during pruning (Han et al. 2014; Rasmussen et al. 2015). We therefore examined whether endocytic, cytoskeletal and/or phagocytic markers also accumulated at sites of epidermal ensheathment. While we observed no enrichment of mature phagocytic markers prior to sheath formation or in mature sheaths, we identified a number of PIP2-linked markers that together provide a

framework for sheath assembly (Table S1). First, we found that a GFP-tagged version of the endocytic adaptor dArf6 was enriched at sites of dendrite ensheathment (Figure 1L-1M). Arf6 regulates clathrin-dependent endocytosis as well as trafficking of recycling endosomes to the plasma membrane (D'Souza-Schorey and Chavrier 2006), and the Arf6 effector phosphatidylinositol4-monophosphate 5-kinase catalyzes plasma membrane synthesis of PIP2 (Honda et al. 1999). Thus, dArf6 and endocytosis may contribute to PIP2 accumulation at sites of sheath formation. Second, we found that a GFP-tagged version of the GTPase Rho1, which promotes filamentous actin (F-actin) assembly, and the F-actin probe GMA-GFP accumulated at sites of epidermal sheath formation (Figure 1N-1Q), consistent with the fact that PIP2 stimulates actin assembly (Yin and Janmey 2003). Finally, in addition to the septate junction marker cora (Figure 1R-1S), which was previously identified as a component of epidermal sheaths (Kim et al. 2012; Tenenbaum et al. 2017), other septate junction markers, including GFP-Neurexin-IV and Neuroglian-GFP, as well as adherens junction markers, including Armadillo-GFP and Shotgun-GFP, *Drosophila* homologues of β -catenin and E-cadherin, respectively, accumulated at epidermal dendrite sheaths (Figure 1T-1U, Figure 1 – figure supplement 1F, Table S1). PIP2 binding regulates membrane association of 4.1R (An et al. 2006) and the maturation of adherens junctions via exocyst-dependent recruitment of E-cadherin (Xiong et al. 2012), thus PIP2 may promote sheath maturation via recruitment of these proteins.

Epidermal sheaths are molecularly similar in the larval skin of *Drosophila* and zebrafish

Sensory axons terminals in the epidermis of zebrafish larvae and adults are ensheathed by the apical membranes of epidermal keratinocytes (Figure 2A) (O'Brien et al. 2012), and ensheathment channels have also been seen in adult fish (Whitewar and Moate 1998; Rasmussen, Vo, and Sagasti 2018). These axonal ensheathment channels are remarkably similar at the ultrastructural level to the channels wrapping somatosensory dendrites in *Drosophila* larvae. By examining the localization of fluorescent reporters for the membrane, cytoskeleton, and cell junctions in basal epidermal cells of zebrafish, we found that zebrafish and *Drosophila* epidermal sheaths are also similar at the molecular level.

At early stages, before sensory axons have grown into the skin, a reporter for PIP2 (PLC^δ-PH-GFP) localized at cell-cell junctions and sparse microdomains near the apical surface (Figure 2B). After axons grew into the skin, PLC^δ-PH-GFP was enriched in continuous, linear apical microdomains, closely associated with axons of both larval zebrafish somatosensory neuron cell types, trigeminal and Rohon-Beard neurons (Figure 2C, H). Farnesylated GFP (CaaX-GFP) similarly localized to microdomains below axons, consistent with the notion that axons are associated with specialized membrane domains in skin cells (Figure 2 – figure supplement 1). Reporters for F-actin (LifeAct-GFP and Utrophin-GFP) were also enriched at these axon-associated domains (Figure 2D, 2E and data not shown), implying that actin may play a role in the morphogenesis of epidermal sheaths.

Electron microscopy of zebrafish epidermal sheaths revealed that autotypic junctions appear to seal the “neck” of these sheaths (O'Brien et al. 2012). To determine the molecular nature of these junctions, we used α-catenin and E-cadherin in-frame,

functional gene traps (Trinh et al. 2011), and a β -catenin antibody to visualize adherens junctions; transiently expressed C-terminally-tagged Desmocollin-like 2 and Desmoplakin BAC reporters to visualize desmosomes; and a gene trap of Jupa [a.k.a. Plakoglobin/ γ -catenin] (Trinh et al. 2011), a protein found in both types of junctions. Reporters for both adherens junction and desmosome proteins localized to apical domains directly above axons, suggesting that both types of junctions associate with epidermal sheaths (Figure 2F-G, I; Figure 2 – figure supplement 1B-F). Consistent with the observation that autotypic junctions are only visible in some TEM images, some of the fluorescent junctional reporters (α -catenin, Jupa) appeared as dotted lines along the length of axons (Figure 2G, Figure 2 –figure supplement 1D), suggesting that they form spot junctions, rather than continuous belts.

Taken together, our results demonstrate similarity in ultrastructure and molecular composition of *Drosophila* and zebrafish epidermal sheaths, suggesting that these structures form via an evolutionarily conserved pathway.

Ensheatment is specific to somatosensory neuron subtypes

To determine if epidermal sheaths are specific to somatosensory neurons in zebrafish, or can occur at any site of axon-basal skin cell contact, we mislocalized axons of another sensory neuron type to the skin. Axons of posterior Lateral Line neurons (pLL) are usually separated from the skin by ensheathing Schwann cells, forming a nerve just internal to the epidermis. Treating animals with an inhibitor of the Neuregulin receptor Erbb3b, which is required for Schwann cell development, causes the entire bundle of pLL axons to directly contact the basal membrane of basal skin cells (Raphael, Perlin,

and Talbot 2010). This treatment created a notable indentation in the basal membrane, but PLC^δ-PH-GFP was not enriched in these domains (Figure 2J, 2K), indicating either that somatosensory axons can uniquely promote the formation of PIP2-rich microdomains, or that only the apical membranes of basal keratinocytes are competent to form these domains.

Next, we examined whether PIP2-rich microdomains formed around all somatosensory neurons or preferentially formed around particular subsets of somatosensory neurons. In *Drosophila* larvae, the vast majority of PLC^δ-PH-GFP-positive sheath structures (94.8 ± 7.8%, n = 8 abdominal hemisegments) were present at sites occupied by c4da sensory dendrites (Figure 3A-3C), yet a subset of PLC^δ-PH-GFP-positive sheaths were not apposed by these dendrites (Figure 1G), suggesting that other classes of da neurons were also ensheathed. To investigate this possibility, we expressed membrane-targeted RFP in different classes of somatosensory neurons and visualized sheaths via epidermal expression of *UAS-PLC^δ-PH-GFP* or anti-cora antibody staining. Among the multi-dendritic da neurons we found that nociceptive c4da neurons exhibited the most extensive ensheathment, mechanosensitive and thermosensitive c3da and c2da neurons exhibited an intermediate level of ensheathment, and proprioceptive c1da neurons exhibited very little ensheathment (Figure 3D-3F). Thus, different morphological and functional classes of somatosensory neurons are ensheathed by the epidermis to different extents.

Although zebrafish somatosensory neurons have not been as clearly categorized into subtypes as *Drosophila* da neurons, similar to *Drosophila*, different individual sensory neurons in zebrafish were ensheathed to different degrees (Figure 3G-3K). The

degree of ensheathment appeared to correlate with axon arbor complexity: axons with fewer branches associated with α -catenin along a greater proportion of their length (up to ~80% axon length) than highly complex axons (<30% axon length). This observation implies that the degree of axon ensheathment may be a subtype-specific feature in zebrafish, like in *Drosophila*.

Sheaths are not pre-patterned in the epidermis

Since epidermal sheaths occur almost exclusively at sites occupied by sensory neurites, we investigated if an epidermal pre-pattern dictates sites of sheath formation or, alternatively, if neuronal signals induce epidermal sheath formation. To differentiate between these possibilities, we first monitored the timing of arrival and distribution of epidermal sheath markers throughout *Drosophila* larval development. Whereas c4da dendrites tile the larval body wall by ~36 hours after egg laying (AEL) (Parrish et al. 2009), PLC ^{δ} -PH-GFP first accumulated in isolated patches adjacent to dendrites at 48 h AEL (Figure 4A-4C, 4G). Epidermal PLC ^{δ} -PH-GFP did not co-occur with large portions of the dendrite arbor until after 96 h AEL (Figure 4D-4F, 4G), a time point when dendrites are internalized in epithelial cells (Jiang et al. 2014, 2018). Furthermore, time-lapse imaging demonstrated that PLC ^{δ} -PH-GFP enrichment at sheaths is not transient; once formed, epidermal sheaths persist or grow, but rarely retract (Figure 4H, Figure 4 – figure supplement 1). Finally, although PLC ^{δ} -PH-GFP and cora extensively co-localized and labeled a nearly identical population of sheaths by the end of larval development (95.7 \pm 5.8 % of cora-positive sheaths are PLC ^{δ} -PH-GFP positive; 88.7 \pm 7.4% of PLC ^{δ} -PH-GFP-positive sheaths are cora-positive; n = 8 hemisegments), cora

accumulation lagged behind PLC δ -PH-GFP (Figure 4G, Figure 4 – figure supplement 2). Thus, although PLC δ -PH-GFP accumulation marks an earlier stage in sheath formation than cora recruitment, we found no evidence that a pre-pattern predicts the site of ensheathment.

In the course of our imaging we occasionally observed hemisegments lacking a c4da neuron. In such cases, epidermal PLC δ -PH-GFP failed to accumulate at sheaths, although PLC δ -PH-GFP accumulation at epithelial cell-cell junctions was comparable to neighboring segments containing c4da neurons, (Figure 4 – figure supplement 3). This observation suggested that dendritic signals induce formation of epidermal sheaths.

Peripheral sensory neurites are required for sheath formation and maintenance

To test the requirement for sensory neurons in epidermal sheath formation we used a genetic cell-killing assay in *Drosophila* to eliminate all c4da neurons and assayed for sheath formation using anti-cora immunostaining. Expressing the pro-apoptotic gene *reaper* in c4da neurons with two copies of the c4da-specific *ppk-Gal4* Gal4 driver (Grueber et al. 2003) resulted in fully penetrant death and clearance of c4da neurons but not other sensory neurons by the end of the first larval instar, prior to appearance of epithelial sheaths. Anti-cora staining of these larvae revealed that although a small number of sheaths were present adjacent to the remaining c2da and c3da neurons, the overall extent of ensheathment was significantly reduced (cora-positive sheath length per mm² of body wall: 2.72 ± 0.64 mm following c4da *reaper* expression, 11.44 ± 1.81 mm in sibling controls without *reaper*; mean \pm sd, n = 8) (Figure 4I-4K). These results demonstrate that dendrite-derived signals induce sheath formation; such signals are

likely short-range signals, as sheaths form at sites directly apposed to dendrites. These results further suggest that modality-specific levels of ensheathment do not reflect competitive interactions between c4da and other da neurons for sheath formation, as the absence of c4da neurons did not potentiate sheath formation in spared neurons.

Next, we investigated the temporal requirement for dendrite-derived signals in epidermal sheath formation. Using a focused laser beam we ablated *Drosophila* c2da, c3da, and c4da neurons at 48 h AEL, prior to appreciable accumulation of sheath markers or appearance of sheaths in TEM sections (Jiang et al. 2014), and assayed for sheath formation at 120 h AEL using anti-cora immunostaining. Following this treatment, cora-positive sheaths did not form (Figure 4L-4N), suggesting that dendrite signals initiate sheath formation after 48 h AEL, the same timeframe when PLC^δ-PH-GFP first accumulates at sites of dendrite contact. These results further demonstrate that different neuron classes have different capacities for ensheathment as removing all of the da neurons that are normally ensheathed did not potentiate c1da neuron ensheathment.

To examine if dendritic signals are likewise required for sheath maintenance we used a focused laser beam to sever the dorsal-anterior dendrites from a c4da neuron at 108 h AEL, after epidermal sheaths had formed, and used time-lapse confocal microscopy to monitor effects on sheath maintenance in larvae expressing the sheath marker *UAS-PLCD-PH-Cerulean* (Figure 4O-4Q). By 12 h post-severing, both the c4da dendrites distal to the cut site and the epidermal sheaths that wrapped them had disappeared (Figure 4R-4T). By contrast, sheaths wrapping the spared dorsal-posterior portion of the c4da dendrite arbor, as well as sheaths that wrapped c2da/c3da neurons

in both the lesioned and unlesioned half of the hemisegment, persisted. Therefore, short-range dendrite-derived signals are required for both the formation and maintenance of epidermal sheaths.

To determine if, as in *Drosophila*, axons are required for the formation of epidermal sheaths in zebrafish, we examined sheath-associated reporters in larvae injected with a morpholino targeting *neurogenin 1* (*neurog1*), a manipulation that blocks somatosensory neuron development (Andermann, Ungos, and Raible 2002; Cornell and Eisen 2002; O'Brien et al. 2012). Basal cells in *neurog1* MO-treated animals lacked coherent PIP2-rich microdomains, apical accumulations of F-actin, and α -catenin-containing autotypic junctions, demonstrating that epidermal sheaths are initiated by axons in zebrafish larvae (Figure 4U-4Z). As in *Drosophila*, axons were also required to maintain sheaths, since PIP2-rich microdomains disappeared soon after laser axotomy and axon degeneration (Figure 4AA).

Zebrafish axonal sheaths and *Drosophila* dendritic sheaths form in a similar sequence

To determine the order of assembly of these sheath-associated proteins we first conducted a series of double-labeling and genetic epistasis analyses in *Drosophila* larvae. We simultaneously expressed the PIP2 marker *UAS-PLC^δ-PH-Cerulean* together with either *UAS-dArf6-GFP* or *UAS-GMA-GFP* in the epidermis of larvae additionally expressing the c4da neuron marker *ppk-CD4-tdTomato* and monitored the timing of arrival of each marker at epidermal sheaths. From the earliest time-point that PIP2 enrichment was detectable at sheaths, we also detected dArf6-GFP enrichment,

albeit at a subset of PLC^δ-PH-Cerulean-positive sheaths, suggesting that dArf6 is recruited to sheaths shortly after PIP2 enrichment (Figure 5A). By contrast, GMA-GFP labeling lagged behind PLC^δ-PH-Cerulean (Figure 5B), appearing on a comparable timescale as cora. Epidermal sheath assembly therefore appears to proceed via separable steps.

Examining ensheathment channel-associated markers at four stages of zebrafish development revealed a similar sequence of events. As in *Drosophila*, we found that membrane reporters appeared near zebrafish axons before F-actin or junctional reporters (Figure 5C). PIP2-rich microdomains frequently apposed axons by 32 hpf, before ensheathment channels were evident ultrastructurally (O'Brien et al. 2012). This observation suggests that the formation of PIP2-positive membrane microdomains is an early step in sheath morphogenesis in zebrafish, as in *Drosophila*. Indeed, time-lapse confocal microscopy demonstrated that these domains formed during development just minutes after an axonal growth cone passed through that region (Figure 5 – figure supplement 1).

To assess the relationship between these sheath-associated proteins, we knocked down lipids or proteins associated with sheaths in *Drosophila*. Specifically, to deplete phosphatidylinositol 4-phosphate and PIP2, we expressed RNAi targeting the phosphatidylinositol 4-kinase gene *PI4KIIIa*; to block endocytosis, we expressed a dominant negative version of *shibire* (*shi*^{DN}), which is defective in GTP binding/hydrolysis (Damke et al. 2001); to block septate junction formation, we expressed *cora*(RNAi) in the epidermis. We found that epidermal *PI4K*(RNAi) and *shi*^{DN} expression severely attenuated PLC^δ-PH-GFP accumulation at sheaths (Figure 5D,

Figure 5 – figure supplement 2). Since PLC^δ-PH-GFP accumulation precedes dArf6 accumulation at the onset of sheath formation, PIP2 accumulation and endocytic events may engage in feed-forward signaling to promote epidermal sheath formation. By contrast, epidermal *cora(RNAi)* had no effect on PLC^δ-PH-GFP accumulation, suggesting that *cora* accumulation is a downstream event in sheath assembly. Consistent with this notion, both epidermal *PI4K(RNAi)* and *shi^{DN}* expression blocked *cora* accumulation at sheaths (Figure 5D, Figure 5 – figure supplement 2), suggesting that *cora* recruitment to sheaths depends on PIP2 accumulation. PIP2 accumulation and *cora* accumulation therefore mark genetically separable steps in sheath assembly that we subsequently refer to as initiation and maturation, respectively (Figure 5E).

Epidermal sheaths regulate dendrite growth dynamics and structural plasticity

What are the functions of epidermal sheaths that wrap somatosensory neurons? Prior studies suggested a role for epidermal ensheathment in restricting dendrite branching in *Drosophila* larvae (Jiang et al. 2014; Tenenbaum et al. 2017). We therefore assayed the requirement in dendrite growth of each of the sheath assembly components we identified in this study. We expressed *PI4K(RNAi)* to reduce epidermal PIP2 levels and monitored effects on c4da dendrite morphogenesis. Compared to controls, epidermis-specific expression of *PI4K(RNAi)* significantly increased the number and decreased the average length of terminal dendrites (Figure 6A-6B, 6G-6H). PLC^δ-PH-GFP can function as a competitive inhibitor of PIP2 signaling (Raucher et al. 2000), and epidermal PLC^δ-PH-GFP expression increased terminal dendrite branch number and decreased dendrite branch length in a dose-dependent manner (Figure 6 – figure supplement 1).

Similarly, blocking epidermal endocytosis via constitutive epidermal expression of *shl*^{DN} or expressing temperature sensitive *shl*^{ts} and using it to conditionally blocking epidermal endocytosis specifically in the time window during which dendrites are normally ensheathed led to severe terminal dendrite branching defects qualitatively similar to *PI4K(RNAi)* (Figure 6C-6D, 6G-6H). Finally, epidermal expression of *cora(RNAi)* induced growth of short terminal dendrites (Figure 6E, 6G-6H) as has been previously reported (Tenenbaum et al. 2017), as did epidermal expression of *shg(RNAi)* (Figure 6F-6H). Thus, blocking the early or late events of epidermal sheath formation deregulates branching morphogenesis of *Drosophila* nociceptive c4da neurons.

To identify the cellular basis of these dendrite growth defects we monitored dendrite dynamics in control or sheath-defective larvae using time-lapse microscopy during the time window when sheaths normally form. Over an 18 h time-lapse beginning at 96 h AEL more than 80% of terminal dendrites persisted in control larvae, with the vast majority of these dendrites elongating (Figure 6I, 6L). By contrast, using epidermis-specific expression of *PI4K(RNAi)* or *cora(RNAi)* to block sheath initiation or maturation, respectively, led to significant alterations in branch dynamics (Figure 6J-6L). First, a larger fraction of terminal dendrites exhibited dynamic growth behavior. Second, the relative levels of growth and retraction were altered; whereas growth predominated in controls, growth and retraction occurred with comparable frequency in *PI4K(RNAi)* and *cora(RNAi)* larvae. Third, the average change in terminal dendrite length was reduced in *PI4K(RNAi)* and *cora(RNAi)* larvae (Figure 6M).

These results suggest that epidermal ensheathment alters dendrite growth properties by stabilizing existing terminal dendrites and promoting their elongation. To

further test this possibility, we simultaneously labeled epidermal sheaths (*Epi>PLC^δ-PH-GFP*) and c4da dendrite arbors (*ppk-CD4-tdTomato*) and monitored terminal dendrite dynamics in ensheathed and unensheathed arbors. Whereas > 65% of terminal dendrites were present only transiently during a 12 h time lapse at the onset of ensheathment (72-84 h AEL), most terminal dendrites persisted during a 12 h time lapse after arbors were extensively ensheathed (108-120 h AEL) (Figure 6N). In this latter time window (108-120 h AEL) we compared the growth dynamics of ensheathed and unensheathed terminal dendrites and found that a significantly higher proportion of ensheathed terminal dendrites were growing or stable over the 12 h time-lapse (Figure 6O). Altogether, our time-lapse imaging results strongly suggest that epidermal sheaths contribute to stabilization of somatosensory dendrites.

What is the relationship between epidermal ensheathment and dendrite branching? While dendrite branch points are occasionally ensheathed (Figure 1B) and new branches can be initiated from ensheathed dendrites (Han et al. 2012), we found that sheath formation is first initiated on long-lived dendrite shafts in proximal portions of the dendrite arbor rather than the more dynamic distal portions of the dendrite arbor (Figure 6 – figure supplement 2) and that dendrite branch points are less extensively ensheathed than unbranched portions of dendrite shafts. We therefore monitored the frequency of dendrite branching from ensheathed and unensheathed portions of dendrite arbors during a 12 h time-lapse. Consistent with prior observations (Han et al. 2012), we did occasionally observe new branch initiation from ensheathed portions of dendrite arbors (Figure 6P), but the majority of new branch initiation occurred on unensheathed portions of dendrites. Intriguingly, a large proportion of new branches

were formed in the vicinity of epithelial intracellular junctions; whether this is simply a result of discontinuities in sheaths at intracellular junctions or reflects the function of non-autonomous branch-promoting activities associated with junctions remains to be determined.

Given that epidermal ensheathment constrains terminal dendrite dynamics in *Drosophila*, we next examined whether epidermal ensheathment limits structural plasticity of dendrite arbors, as has been suggested (Parrish et al. 2009; Jiang et al. 2014). Embryonic ablation of c4da neurons leads to exuberant dendrite growth in spared neurons beyond their normal boundaries to fill vacated territory (Grueber et al. 2003; Sugimura et al. 2003). This capacity of c4da neurons to expand their dendrite arbors beyond normal boundaries is progressively limited during development, concomitant with the increase in epidermal dendrite ensheathment (Parrish et al. 2009; Jiang et al. 2014). Following ablation of a single c4da neuron at 72 h AEL, the spared neighboring neurons extend their dendrite arbors to cover 13% of the vacated territory, on average (Figure 6Q, 6T). If epithelial ensheathment limits the structural plasticity of c4da dendrite arbors, we reasoned that blocking epithelial sheath formation should potentiate the invasive growth activity of c4da neurons following ablation of their neighbors. Indeed, epidermis-specific *PI4K(RNAi)* or *cora(RNAi)* resulted in a significant potentiation of dendrite invasion (Figure 6R-6T). In addition to regulating the growth dynamics and elongation of individual terminal dendrites, these results suggest that epidermal ensheathment contributes to the fidelity of receptive field coverage by coupling dendrite and epidermis expansion.

Epidermal sheaths regulate nociception in *Drosophila* larvae

What role, if any, does epidermal ensheathment play in somatosensation? Having found that nociceptive c4da neurons and proprioceptive c1da neurons were the most extensively and least extensively ensheathed da neurons, respectively, we investigated whether blocking sheath formation affected sensory-evoked behavioral responses regulated by these neurons. Harsh touch activates c4da nociceptive neurons to elicit stereotyped nocifensive rolling responses (Zhong et al., 2010), so we monitored touch-evoked rolling responses and rates of larval locomotion in control or sheath-defective larvae as a measure for sheath influence on c4da neuron function. Stimulation with a 78nM von Frey filament induced nociceptive rolling behavior in >60% of control larvae, whereas c4da-specific expression of the inward rectifying potassium channel Kir2.1 strongly attenuated this rolling response (Figure 7A). Compared to controls, epidermal expression of either *PI4KIIIa(RNAi)* to block PIP2 accumulation or *PIS(RNAi)* to reduce phosphoinositol biosynthesis, or feeding larvae the cell permeant polyphosphoinositide-binding peptide PBP10 to antagonize PIP2 signaling during the time window of sheath formation significantly attenuated mechanonociceptive behavior (Figure 7A). Epidermal expression of *shi^{DN}* to block epidermal endocytosis and *cora(RNAi)* to block sheath maturation similarly attenuated mechanonociception. We additionally found that previously reported treatments that block ensheathment including overexpressing α - and β -integrin in c4da neurons to tether dendrites to the ECM (Han et al. 2012; Jiang et al. 2014) and mutation of the miRNA *bantam* (Jiang et al. 2014) displayed reduced rolling rates in response to von Frey stimuli.

Finally, we assayed for effects of ensheathment on larval locomotion. Input from proprioceptive c1da neurons is required for coordinated larval locomotion, and perturbing c1da neuron function severely attenuates larval crawling speed (Song et al. 2007). Treatments that reduced epidermal sheath formation did not reduce larval stride length or crawling speed as would be expected for disruption of proprioceptor function, but instead led to increased larval crawling speed (Fig. 7B and data not shown). This increased crawling speed was largely the result of reduced turning frequency and a concomitant increase in forward-directed locomotion (Fig. 7C), similar to defects in crawling trajectory induced by perturbing c4da function (Ainsley et al. 2003; Gorczyca et al. 2014), further suggesting that ensheathment modulates c4da function. Thus, epidermal ensheathment potentiates nociceptive mechanosensory responses and is apparently dispensable for proprioceptor function, consistent with our observation that nociceptive c4da but not proprioceptive c1da neurons exhibit extensive epidermal ensheathment.

Discussion

A neuron's function is profoundly influenced by its interaction with cells around it. In the skin, specialized interactions with epidermal cells influence the function of a variety of different sensory neurons. However, despite the fact that keratinocytes are the most abundant cell type in the epidermis, roles for keratinocyte-sensory neuron interactions in somatosensation are still not well characterized. Here, we have identified a conserved morphogenetic program for ensheathment of peripheral somatosensory neurites by keratinocytes. In both *Drosophila* and zebrafish, sensory neurite-derived signals induce

keratinocytes or keratinocyte-like epidermal cells to ensheath somatosensory neurons in a neuron type-specific manner. These neurite-derived signals induce local formation of epidermal PIP2-enriched membrane microdomains that are essential for ensheathment, local assembly of F-actin, and recruitment of junctional proteins that likely seal the sheaths. (Similarities and differences (timescale) in fly and fish ensheathment)

What triggers the formation of epidermal sheaths?

While the signals are not yet known, our studies define key features of the signaling system that drives sheath formation. First, epidermal sheath formation likely relies on short-range, contact-mediated signals involving neuron-expressed ligands and epidermal receptors, as sheaths form exclusively at sites occupied by peripheral sensory neurites. Such a signaling system bears similarity to the *C. elegans* epidermal SAX-7/L1CAM and MNR-1/Menorin co-ligand complex that interacts with neuronal DMA-1 to regulate patterning of PVD dendrites (Dong et al. 2013; Salzberg et al. 2013). However, whereas PVD dendrites are positioned according to a hypodermal grid of SAX-7/L1CAM expression (Liang et al. 2015), the location of epidermal sheaths is dependent on neuron-derived signals rather than an epidermal pre-pattern. Second, different types of neurons have different capacities to induce epidermal sheath formation; in zebrafish, only somatosensory neurons are capable of inducing sheath formation on the apical membranes of basal keratinocytes, and different classes of somatosensory neurons are ensheathed to different degrees in *Drosophila* and zebrafish. The epidermal sheaths that wrap different types of somatosensory neurons

are structurally similar, thus it seems likely that different levels of the sheath-inducing ligand determine the extent of ensheathment much as Nrg1 levels can drive the extent of Schwann cell ensheatment (Michailov et al. 2004). Based on the conservation in the molecular machinery of sheath formation, such a ligand and its epidermal receptor are likely conserved in fish and flies. Third, sheath formation is temporally regulated. In both *Drosophila* and zebrafish, flies, somatosensory neurites innervate the epidermis more than a day prior to sheath formation (Parrish et al. 2009; O'Brien et al. 2012). This may reflect a lack of competence by epithelial cells to ensheath somatosensory neurites as accelerating developmental progression in the *Drosophila* epidermis leads to precocious dendrite ensheathment (Jiang et al. 2014). Finally, our laser severing experiments suggest that peripheral neurites are required to maintain epidermal sheaths. Whether maintenance of sheaths is dependent on a dedicated maintenance signal or simply reflects the absence of morphogenetic signals that would remodel sheaths, for example the exposure by neurites to phosphatidylserine or other engulfment-promoting signals, remains to be determined.

The earliest epidermal morphogenetic event we identified downstream of neurite-derived ensheathment signals is the appearance of PIP2-enriched membrane microdomains. How might neurite-derived signals trigger local accumulation of epidermal PIP2? Two prominent mechanisms exist to form localized pools of PIP2 in the plasma membrane (Kwiatkowska 2010), and each can be triggered by cell-cell contacts. First, PIP2 can be locally clustered via electrostatic interactions with polybasic proteins such as myristoylated alanine rich C-kinase substrate (MARCKS) (Glaser et al. 1996; Gambhir et al. 2004; McLaughlin and Murray 2005), which additionally binds and

cross-links filamentous actin (Myat et al. 1997). Protocadherins regulate cortical dendrite morphogenesis in part by maintaining a membrane-associated pool of active MARCKS (Garrett et al. 2012), thus Protocadherin-based adhesion provides one potential mechanism for localizing MARCKS and hence PIP2 in epidermal cells. Neuronal signals could likewise trigger PIP2 localization via engagement of transmembrane receptors with intracellular domains that electrostatically interact with and cluster PIP2 (McLaughlin and Murray 2005) or via membrane recruitment of other polybasic proteins such as Adducins or GAP43 (Kwiatkowska 2010). Second, PIP2 can be locally synthesized, most commonly via phosphorylation of phosphatidylinositol 4-phosphate, and type I phosphatidylinositol 4-phosphate 5 kinase (PIP5KI) can associate with N-cadherin to locally produce PIP2 at sites of N-cadherin adhesion (El Sayegh et al. 2007). PIP5Kly associates with the exocyst via direct interaction with Exo70 to promote membrane targeting of E-cadherin (Xiong et al. 2012), thus cadherin-based adhesion can be both a cause and effect of localized PIP2 synthesis. While we have not found evidence for an epidermal PIP2 pre-pattern that determines sites of ensheathment, PIP5K additionally localizes to focal adhesions to provide a local source of PIP2 (Ling et al. 2002). Thus, it will be intriguing to determine whether Integrin-based adhesions contribute to epidermal sheath formation by generating local asymmetries in PIP2 levels that get amplified by neuron-derived signals.

Plasma membrane enrichment of epidermal PIP2 serves as a critical control point for a variety of cellular processes (Sun et al. 2013). Among these, we note remarkable similarities between epidermal sheath formation and the early events of phagocytosis. First, sheath formation and the early stages of phagocytosis appear to involve similar

cellular rearrangements, with ensheathing cells and engulfing cells wrapping their targets with membrane protrusions. Second sheath formation and phagocytosis share a common set of molecular mediators as PIP2 accumulates in nascent epidermal sheaths and in the phagocytic cup of engulfing cells (Botelho et al. 2000), as does a network of F-actin (Scott et al. 2005). Third, many types of ensheathing cells additionally exhibit phagocytic activity, including *Drosophila* and zebrafish keratinocytes (Han et al. 2014; Rasmussen et al. 2015), *Drosophila* ensheathing glia (Doherty et al. 2009), and astrocytes (Chung et al. 2013). However, whereas PIP2 levels persist at sheaths, PIP2 disappears from the phagosomal membrane during the late stages of phagocytosis (Botelho et al. 2000), leading to disassembly of the associated actin network (Scott et al. 2005). Similarly, transient accumulation of PIP2 is a feature of endocytosis, cell migration, and other PIP2 regulated morphogenetic events. Thus, it seems plausible that reducing PIP2 levels leads to phagocytic engulfment of neurites, providing a mechanism for rapid conversion of the epidermal ensheathment channels to engulfment channels; such a finding could account for the finding that *Drosophila* epidermal cells actively participate in dendrite fragmentation (Han et al. 2014).

Functional roles for epidermal neurite ensheathment

Consistent with prior reports, we found that epidermal ensheathment limits dendrite branching of *Drosophila* nociceptive c4da neurons (Jiang et al. 2014; Tenenbaum et al. 2017). We also found that the extent of ensheathment is inversely related to peripheral axon branch number in zebrafish somatosensory neurons, suggesting that epidermal ensheathment could similarly regulate neurite branching in vertebrates. This epidermal

growth control of peripheral sensory arbors appears to involve two related mechanisms. First, epidermal ensheathment limits dendrite branching; dendrite branching events rarely occur on ensheathed dendrites, and blocking epidermal ensheathment potentiates dendrite branching. This dendrite branching control may reflect a masking of dendrite arbors from substrate-derived signals that promote branching or a steric hindrance of branching. Second, epidermal ensheathment stabilizes existing neurites; blocking epidermal ensheathment potentiates dynamic growth behavior and structural plasticity in *Drosophila* sensory neurons. Determining whether ensheathment similarly regulates structural plasticity in zebrafish will require development of more and better tools for effectively blocking sheath formation in zebrafish. However, given that the timing of epidermal sheath formation correlates with the developmental restriction in structural plasticity in both *Drosophila* and zebrafish (O'Brien et al. 2012; Jiang et al. 2014), developmental control of ensheathment appears to be a likely mechanism to stabilize receptive fields of somatosensory neurons.

Different types of somatosensory neurons appear to be ensheathed to different degrees. What would be the purpose of such an arrangement? Many different types of somatosensory neurons innervate overlapping territories, and one recent study suggests that selective ensheathment of particular sensory neuron types facilitates coexistence of different types of sensory neurons in a given territory (Tenenbaum et al. 2017). Differential levels of ensheathment may additionally allow for differential coupling of somatosensory neurons to epidermal growth-promoting signals. Likewise, differential ensheathment of somatosensory neuron types may allow different levels of functional coupling of sensory neurons and epidermis. Our finding that nociceptive c4da neurons

are the most extensively ensheathed *Drosophila* somatosensory neurons, and that ensheathment regulates nociceptive sensitivity, suggests that epidermal ensheathment may play a particularly important role in tuning responses to noxious stimuli. Intriguingly, mutations that block ensheathment impair the function of a subset of *C. elegans* mechanosensory neurons (X. Chen and Chalfie 2014); whether these mechanosensory impairments are a consequence of ensheathment defects or other effects of the mutations remains to be determined.

How might epidermal sheaths influence nociceptive sensitivity? First, epidermal sheaths may potentiate the functional coupling of epidermal cells to somatosensory neurons. Recent studies suggest that sensory-evoked responses of keratinocytes may modulate sensory neuron function (Koizumi et al. 2004; Baumbauer et al. 2015; Pang et al. 2015; Moehring et al. 2018), and epidermal sheaths could provide sites for vesicle release from keratinocytes or direct electrical coupling between keratinocytes and somatosensory neurons. Merkel cells provide a precedent for the former possibility (Maksimovic, Baba, and Lumpkin 2013), but whether keratinocytes possess presynaptic release machinery and which neurotransmitters they express remain to be determined. Alternatively, epidermal ensheathment could potentiate nociceptor sensitivity by increasing proximity to stimulus source, by clustering sensory channels, or by some other means. Regardless of the mechanism, our findings that epidermal ensheathment modulates nociceptive sensitivity suggest that defects in epidermal ensheathment could contribute to sensory deficits in human disease. Intriguingly, some forms of peripheral neuropathy exhibit loss of unmyelinated intraepidermal nerves (Weis et al. 2011;

Üçeyler et al. 2013); whether defects in epithelial ensheathment play a role in these sensory neuropathies remains to be determined.

Materials and Methods

Animal Care

Flies were maintained on standard cornmeal-molasses-agar media and reared at 25° C under 12 h alternating light-dark cycles. The following alleles were used in this study: *w¹¹¹⁸* (BDSC:); *ppk-CD4-tdTomato* (BDSC:35844, BDSC:35845); *ppk-mCD8-GFP* (Han, Jan, and Jan 2011); *UAS-PLCγ-PH-GFP* (BDSC:39693); *UAS-PLCγ-PH^{S39R}-GFP* (BDSC:39694); *UAS-PLCD1-PH-Cerulean* (BDSC:31421); *UAS-2xOsh2PH-GFP* (BDSC:57353); *UAS-GMA-GFP* (BDSC:31176); *UAS-Rho1-GFP* (BDSC:9393); *UAS-shg-GFP* (BDSC:58445); *UAS-Arf51-GFP* (BDSC:65867); *UAS-CD4-tdGFP* (BDSC:35836); *lexAOP-CD4-tdTomato* (BDSC:77138); *UAS-PIS(RNAi)* (BDSC:29383); *UAS-PI4KII(RNAi)* (BDSC:38242); *UAS-cora(RNAi)* (BDSC:51845); *UAS-shg(RNAi)* (BDSC:32904); *UAS-shi^{ts}* (BDSC:44222); *UAS-shi^{DN}* (BDSC:5811); *UAS-rpr* (BDSC:5824); *UAS-mys*, *UAS-mew* (Jiang et al. 2014); *UAS-Kir2.1-GFP* (BDSC:6596); *A58-Gal4* (BDSC:); *ppk-Gal4* (Grueber et al. 2003); *21-7-Gal4* (Song et al. 2007); *Cha^{7.4kb}-Gal80* (Sakai et al. 2009); *elav-LexA* (BDSC:23872); *nompC-LexA* (BDSC:52241); *bantam^{Δ1}* (Brennecke et al. 2003); *Arf51^{GFP}* (BDSC:60586); *shg^{GFP}* (BDSC:60584). See Table S1 for a complete list of reporters used for the expression screen detailed in Figure 1 and Figure 1 – figure supplement 1. Experimental genotypes are listed in Table S2.

704 *Zebrafish*

705 Zebrafish (*Danio rerio*) were grown at 28.5°C on a 14 h/10 h light/dark cycle. The
 706 following previously described transgenic strains were used: *TgBAC(tp63:GAL4FF)^{la213}*,
 707 *Tg(isl1[ss]: LEXA-VP16,LEXAop:tdTomato)^{la215}* (Rasmussen et al. 2015), *Tg(isl1:GAL4-*
 708 *VP16,UAS:RFP)^{zf234}* (O'Brien, Martin, et al. 2009), *Gt(ctnna-citrine)^{ct3a}* (Trinh et al.
 709 2011), *Gt(jupa-citrine)^{ct520a}* (Trinh et al. 2011), *Tg(UAS:lifeact-GFP)^{mu271}* (Helker et al.
 710 2013) and *Tg(UAS:GFP-CAAX)^{pd1025}* (Ellis, Bagwell, and Bagnat 2013). All
 711 experimental procedures were approved by the Chancellor's Animal Research Care
 712 Committee at UCLA.

713

714 *BAC modification*

715 To generate BAC reporters for *dsc2l* and *dspa*, the corresponding stop codons in BACs
 716 CH73-316A13 and CH211-120J4, respectively, were replaced by a GFP-KanR cassette
 717 as previously described (Suster et al. 2011).

718

719 *UAS:GFP-PH-PLC zebrafish transgenic ilne construction*

720 To generate pME-EGFP-PH-PLC, the PH domain of rat PLC1 δ 1 was PCR amplified
 721 from pAA173 (Kachur, Audhya, and Pilgrim 2008) and cloned into pME-EGFP (Kwan et
 722 al. 2007) using the restriction enzymes XhoI and BglII. The pDEST-4xUASnr-EGFP-PH-
 723 PLC-pA plasmid was created by Gateway cloning of p5E-4xUASnr (Akitake et al. 2011),
 724 pME-EGFP-PH-PLC and p3E-pA. To create a stable line, one cell stage embryos were

injected with pDEST-4xUASnr-EGFP-PH-PLC-pA and *tol2* mRNA, raised to adulthood and screened for transgene transmission to the F1 generation.

Zebrafish Cdh1-tdtomato^{xt18} gene trap

E-cadherin knock-in fish lines were made by the approach developed by Auer et al. (Auer et al. 2014). Zebrafish were injected at the 1-cell stage with Cas9 mRNA and two gRNAs – one targeting E-cadherin 3 amino acids upstream of the stop codon, and one targeting GFP in a coinjected plasmid (pUC19 GFPgRNA-Tomato-Ub polyA) containing the tdTomato ORF. This causes the insertion of the entire pUC19 GFPgRNA-Tomato-Ub polyA sequence, starting at the GFP gRNA site directly upstream of the Tomato ORF. ~1 nl of an injection mix consisted of 50 ng/μl of each gRNAs, pUC19 GFPgRNA-Tomato-Ub at 12 ng/μl, and Cas9 mRNA at 150 ng/μl. Animals with fluorescence at 2 dpf were raised to adulthood and outcrossed to identify founder animals. An insertion allele was identified in which the two penultimate residues, glycine and a glutamate, were deleted during NHEJ insertion, but the final amino acid, aspartate, was rescued with sequence from the insertion. The c-terminus of E-cadherin thus changed from GGGED to GGD, with the tdTomato sequence fused directly downstream.

Zebrafish transient transgenesis

To label lateral line axons, one to four-cell stage zebrafish embryos were injected with 25 pg of a *neurod:mTangerine* plasmid (gift from Alex Nechiporuk, Oregon Health &

Science University, Portland, OR). 200 pg of BAC reporters for *dsc2l* and *dspa* were injected at the one to four-cell stage.

Morpholino injection

To block somatosensory neuron development, one cell stage embryos were injected with 1 nl of injection mixture containing an antisense morpholino oligonucleotide targeting *neurog1* (5'-ACGATCTCCATTGTTGATAACCTGG-3') at a concentration of 0.7 mM (Andermann, Ungos, and Raible 2002; Cornell and Eisen 2002). Loss of response to touch was monitored to confirm efficacy of the treatment. As a control, embryos were injected with 1 nl of an antisense morpholino that targets an intron of the human beta-globin gene (5'-CCTCTTACCTCAGTTACAATTTATA-3') at a concentration of 0.7 mM. Antisense morpholino oligonucleotides were synthesized by GeneTools (Philomath, OR).

AG1478 treatment

The ErbB receptor antagonist AG1478 was used to perturb repositioning of the pLLn below the epidermis (Raphael, Perlin, and Talbot 2010). Embryos were bathed in embryonic medium containing either 4 μ M AG1478/1% DMSO or 1% DMSO as a control.

Microscopy

Imaging. *Drosophila* larvae were mounted in 90% glycerol under No. 1 coverslips and imaged using a Leica SP5 microscope with a 40× 1.2 NA oil immersion lens. For time-lapse analysis, larvae were imaged at the indicated time, recovered to yeasted agar plates with vented lids, aged at 25°C, and imaged again. Zebrafish embryos were mounted as described (O'Brien, Rieger, et al. 2009). Confocal imaging was performed on an LSM 510 or 800 confocal microscope (Carl Zeiss).

Laser ablation. Larvae were mounted in 90% glycerol under No. 1 coverslips, dendrites were imaged using a Leica SP8 2-photon microscope with a 20x 1.0 NA water immersion lens at 2x magnification under low (<20%) laser power. Cells were ablated or dendrites were severed by focusing high laser output (>80%) on the nucleus or a ~2 micron dendrite segment (64x magnification ROI scan), respectively. Larvae were recovered to yeasted agar plates with vented lids, aged at 25°C, and processed for live imaging or immunostaining at the indicated time. Zebrafish axons were severed using a 2-photon laser as previously described (O'Brien, Rieger, et al. 2009).

Drosophila Immunostaining. Third instar larvae were pinned on a sylgard plate, filleted along the ventral midline, and pinned open. After removing the intestines, fat bodies, imaginal discs and ventral nerve cord, fillets were fixed in PBS with 4% PFA for 15 min at room temperature, washed 4 times for 5 min each in PBS with 0.3% Tx-100 (PBS-Tx), blocked for 1 h in PBS-Tx + 5% normal donkey serum, and incubated in primary antibody overnight at 4° C. Samples were washed 4 times for 5 min each in PBS-Tx,

incubated in secondary antibody for 4 h at room temperature, washed 4 times for 5 min each in PBS-Tx, and stored in PBS prior to imaging. Antibody dilutions were as follows: rabbit anti-GFP (Fisher #A-11122, 1:500), mouse anti-coracle (DSHB, C566.9 supernatant, 1:25), Rabbit anti-dsRed (Clontech #632496, 1:200), HRP-Cy5 (Jackson Immunoresearch, 1:100), Goat anti-Mouse Alexa488 (Thermofisher A-11001, 1:200), Goat anti-rabbit Alexa 488 (Thermofisher A-11034, 1:200), Goat anti-rabbit Alexa 555 (Thermofisher A-21428, 1:200).

Drosophila expansion microscopy

Immunostaining was as above with the following antibodies: Mouse anti-GFP, clone 3E6 (Invitrogen #A11120, 1:100), Rabbit anti-dsRed (Clontech #632496, 1:50), Goat anti-Mouse Alexa488 (Thermofisher A31561, 1:100), Donkey anti-Rabbit ATTO 565 (Vaughan lab, 1:10). Following immunostaining, samples were mounted on lysine-coated #1.5 cover glass in polydimethylsiloxane wells and incubated in monomer solution (2 M NaCl, 8.625% Sodium Acrylate, 2.5% Acrylamide, 0.15% Bisacrylamide in PBS) for 1 h at 4° C prior to gelation. A stock of 4-hydroxy-2,2,6,6-tetramethylpiperidin-1-oxyl (4-hydroxy-TEMPO) at 1% (wt/wt) in water was added to the incubation solution and diluted to concentration of 0.01%. Concentrated stocks of tetramethylethylenediamine (TEMED) and ammonium persulfate (APS) at 10% (wt/wt) in water were added sequentially to the incubation solution and diluted to concentrations of 0.2% (wt/wt). The tissues were then incubated at 37 °C for 3-4 h. After gelation, the gels were cut and placed in a small 12-well chamber and 1mg/ml of Chitinase in PBS (pH 6.0) was used to digest the cuticles for ~4 d at 37 °C. Chitinase-treated samples

were incubated with 1000 units/ml collagenase solution (prepared with buffer 1x HBSS lacking calcium, magnesium, and phenol red) with 0.01 M CaCl_2 and 0.01 M MgCl_2 overnight in a 37 °C shaking incubation chamber. Samples were then rinsed with PBS twice for 5 min and digested in 8 units/ml proteinase K solution in digestion buffer (40 mM Tris pH 8.0, 1 mM EDTA, 0.5% Triton, 0.8 M Guanidine HCl) for 1 h at 37 °C. Subsequently, samples were removed from the digestion solution and were allowed to expand overnight in a large excess of deionized water. After expansion, the expanded gel was trimmed to fit onto the coverglass, excess water was removed, and the gel was mounted on a lysine-coated cover glass for imaging. Confocal microscopy was performed on a Leica SP5 inverted confocal scanning microscope using a 63x 1.2 NA water lens.

Drosophila SBF-SEM

Third instar larva were perforated with insect pins and cut open on ice in freshly made fixative (2.5% glutaraldehyde, 4% paraformaldehyde, 0.1 M sodium cacodylate). Samples were centrifuged 15000 x rpm in a microcentrifuge for 1 h and then incubated at 4° C overnight to achieve thorough fixation. Next, samples were washed 5 times for 5 min each in 0.1 M sodium cacodylate and then post-fixed in osmium ferrocyanide for 1 h on ice. The tissues were then washed 5 times for 5 min each in ddH₂O at room temperature and incubated in a 1% thiocarbohydrazide solution for 20 min at room temperature. The samples were washed 5 times for 5 min each in ddH₂O at room temperature and then incubated in 2% osmium tetroxide for 30 min at room temperature. Following another 5 washes for 5 min each in ddH₂O at room temperature,

samples were stained en bloc in 1% uranyl acetate at 4° C overnight. The following day, tissues were washed 5 times for 5 min each in ddH₂O at room temperature and stained en bloc in Walton's lead aspartate for 30 min at 60° C. The samples were then washed 5 times for 5 min each in ddH₂O and dehydrated in an ice cold ethanol series (30%, 50%, 70%, and 95% EtOH), then transferred to room temperature for 5 min. This was followed by 2 changes of 100% EtOH and 2 changes of propylene oxide for 5 min each. The tissues were then infiltrated in a 1:1 mixture of propylene oxide : Durcupan resin, for 2 h at room temperature followed by overnight infiltration in fresh Durcupan. The following day, tissues were given a fresh change of Durcupan for 2 h at room temperature and then placed in flat embedding molds and polymerized in a 60° C oven for two days. The blocks were trimmed and imaged using a Zeiss Sigma scanning electron microscope with a Gatan 3-view system at 2.5-1.7 KV. Stacks (1000 sections) were collected with a 60 nm step size.

Zebrafish immunostaining

Embryos were stained with a mouse anti- β -catenin antibody (610153; BD Biosciences) as previously described (Rasmussen et al. 2015).

Morphometric analysis

All image analysis was performed using Fiji (Schindelin et al. 2012). The Simple Neurite Tracer plugin (Longair, Baker, and Armstrong 2011) was used to trace neurites, ensheathment channels and cell borders. Only basal cells for which the entire perimeter

of the cell was visible were traced. R (<https://www.r-project.org/>) was used to generate plots and perform statistical tests.

Behavior assays

Harsh Touch. Larvae were placed in a plastic petri dish with enough water, so larvae remained moist, but did not float in the dish. Von frey filaments made from fishing line and affixed to glass capillaries were applied to the dorsal side of the larvae between segments A3-A6 until the filament buckled, exhibiting a pre-determined force (~78mN). A positive response was scored if one complete nocifensive roll occurred within 10 sec of the mechanical stimulus.

Larval locomotion. Larvae were washed and placed on a 2% agar plate. To measure crawling velocity, 10 second videos of individual crawling larvae were recorded as uncompressed avi files using a Leica DFC310 FX camera on an AmScope FMA050 mount. Files were converted to flymovieformat with any2ufmf and analyzed in Ctrax (Branson et al. 2009). To measure crawling trajectory, larval locomotion was analyzed using the frustrated total internal reflection-based imaging method FIM together with the FIMTrack software package (Risse et al. 2013).

Experimental Design and Statistical Analysis

Datasets were tested for normality using Shapiro-Wilks goodness of fit tests. Details on statistical tests are provided in figure legends.

Acknowledgements

This work was supported by grants from the National Institutes of Health To J.Z.P. (NINDS R01 NS076614), AS (NIAMS R01 AR064582), J.P.R. (NICHD K99 HD086271), and J.C.V. (NIMH R01 MH115767), a JSPS long-term fellowship and startup funds from UW (J.Z.P); a WRF-Hall fellowship (K.P.L); a Jane Coffin Childs Memorial Fund fellowship. Fly Stocks were obtained from the Bloomington *Drosophila* Stock Center (NIH P40OD018537) and antibodies were obtained from the Developmental Studies Hybridoma bank, created by the NICHD of the NIH and maintained at The University of Iowa, were used in this study. We thank Julie Brill, Kazuo Emoto, and Peter Soba for helpful discussions, Le Trinh and Michel Bagnat for fish lines and Vasudha Chauhan for BAC cloning, and Stephen Basenfelder and Son Giang for excellent fish care.

Author Contributions

Conception and design: *Drosophila* studies, N.J. and J.Z.P; zebrafish studies, J.P.R. and A.S.

Acquisition of *Drosophila* data: SEM, N.J. and E.P.; ExM, N.J., H.J.K. and J.C.V.; marker screen, N.J. and J.Z.P.; ablation studies, N.J. and J.Z.P.; time-lapse imaging, J.Z.P.; behavior analysis, K.P.L. and J.Z.P.

Acquisition of zebrafish data: J.P.R., J.A.C., M.F.R. and A.S.

Generation of *E-cadherin-tdTomato*: M.R.C.

Analysis and Interpretation of *Drosophila* data: epidermis imaging data, N.J. and J.P; dendrite imaging and larval behavior data, J.P.

Analysis and Interpretation of zebrafish data: J.P.R., J.A.C., M.F.R. and A.S.

Drafting the article: J.Z.P., A.S., and J.P.R.

Declaration of Interests

The authors declare no competing interests.

References

- Ainsley, Joshua A., Janette M. Pettus, Dmitry Bosenko, Clare E. Gerstein, Natalya Zinkevich, Michael G. Anderson, Christopher M. Adams, Michael J. Welsh, and Wayne A. Johnson. 2003. "Enhanced Locomotion Caused by Loss of the Drosophila DEG/ENaC Protein Pickpocket1." *Current Biology* 13 (17): 1557–63.
- Akitake, Courtney M., Michelle Macurak, Marnie E. Halpern, and Mary G. Goll. 2011. "Transgenerational Analysis of Transcriptional Silencing in Zebrafish." *Developmental Biology* 352 (2): 191–201. <https://doi.org/10.1016/j.ydbio.2011.01.002>.
- An, Xiuli, Xihui Zhang, Gargi Debnath, Anthony J. Baines, and Narla Mohandas. 2006. "Phosphatidylinositol-4,5-Biphosphate (PIP2) Differentially Regulates the Interaction of Human Erythrocyte Protein 4.1 (4.1R) with Membrane Proteins." *Biochemistry* 45 (18): 5725–32. <https://doi.org/10.1021/bi060015v>.
- Andermann, Peter, Josette Ungos, and David W. Raible. 2002. "Neurogenin1 Defines Zebrafish Cranial Sensory Ganglia Precursors." *Developmental Biology* 251 (1): 45–58.
- Auer, Thomas O., Karine Duroure, Anne De Cian, Jean-Paul Concordet, and Filippo Del Bene. 2014. "Highly Efficient CRISPR/Cas9-Mediated Knock-in in Zebrafish by Homology-Independent DNA Repair." *Genome Research* 24 (1): 142–53. <https://doi.org/10.1101/gr.161638.113>.
- Baumbauer, Kyle M., Jennifer J. DeBerry, Peter C. Adelman, Richard H. Miller, Junichi Hachisuka, Kuan Hsien Lee, Sarah E. Ross, H. Richard Koerber, Brian M. Davis, and Kathryn M. Albers. 2015. "Keratinocytes Can Modulate and Directly Initiate Nociceptive Responses." *ELife* 4. <https://doi.org/10.7554/eLife.09674>.
- Bidaux, Gabriel, Anne-sophie Borowiec, Dmitri Gordienko, Benjamin Beck, George G. Shapovalov, Loïc Lemonnier, Matthieu Flourakis, et al. 2015. "Epidermal TRPM8 Channel Isoform Controls the Balance between Keratinocyte Proliferation and Differentiation in a Cold-Dependent Manner." *Proceedings of the National Academy*

- of Sciences of the United States of America 112 (26): E3345-3354.
<https://doi.org/10.1073/pnas.1423357112>.
- Botelho, R. J., M. Teruel, R. Dierckman, R. Anderson, A. Wells, J. D. York, T. Meyer, and S. Grinstein. 2000. "Localized Biphasic Changes in Phosphatidylinositol-4,5-Bisphosphate at Sites of Phagocytosis." *The Journal of Cell Biology* 151 (7): 1353-68.
- Branson, Kristin, Alice Robie, John Bender, Pietro Perona, and Michael Dickinson. 2009. "High-Throughput Ethomics in Large Groups of *Drosophila*." *Nature Methods* 6 (6): 451-57. <https://doi.org/10.1038/nmeth.1328>.
- Brennecke, Julius, David R Hipfner, Alexander Stark, Robert B Russell, and Stephen M Cohen. 2003. "Bantam Encodes a Developmentally Regulated MicroRNA That Controls Cell Proliferation and Regulates the Proapoptotic Gene Hid in *Drosophila*." *Cell* 113 (1): 25-36.
- Cauna, N. 1973. "The Free Penicillate Nerve Endings of the Human Hairy Skin." *Journal of Anatomy* 115 (Pt 2): 277-88.
- Chalfie, M., and J. Sulston. 1981. "Developmental Genetics of the Mechanosensory Neurons of *Caenorhabditis Elegans*." *Developmental Biology* 82 (2): 358-70.
- Chen, Suzhen, Carlos Rio, Ru-Rong Ji, Pieter Dikkes, Richard E. Coggeshall, Clifford J. Woolf, and Gabriel Corfas. 2003. "Disruption of ErbB Receptor Signaling in Adult Non-Myelinating Schwann Cells Causes Progressive Sensory Loss." *Nature Neuroscience* 6 (11): 1186-93. <https://doi.org/10.1038/nn1139>.
- Chen, Xiaoyin, and Martin Chalfie. 2014. "Modulation of *C. Elegans* Touch Sensitivity Is Integrated at Multiple Levels." *The Journal of Neuroscience: The Official Journal of the Society for Neuroscience* 34 (19): 6522-36.
<https://doi.org/10.1523/JNEUROSCI.0022-14.2014>.
- Chen, Yong, Quan Fang, Zilong Wang, Jennifer Y. Zhang, Amanda S. MacLeod, Russell P. Hall, and Wolfgang B. Liedtke. 2016. "Transient Receptor Potential Vanilloid 4 Ion Channel Functions as a Pruriceptor in Epidermal Keratinocytes to Evoke Histaminergic Itch." *The Journal of Biological Chemistry* 291 (19): 10252-62.
<https://doi.org/10.1074/jbc.M116.716464>.
- Chung, Won-Suk, Laura E. Clarke, Gordon X. Wang, Benjamin K. Stafford, Alexander Sher, Chandrani Chakraborty, Julia Joung, et al. 2013. "Astrocytes Mediate Synapse Elimination through MEGF10 and MERTK Pathways." *Nature* 504 (7480): 394-400.
<https://doi.org/10.1038/nature12776>.
- Cornell, Robert A., and Judith S. Eisen. 2002. "Delta/Notch Signaling Promotes Formation of Zebrafish Neural Crest by Repressing Neurogenin 1 Function." *Development* 129 (11): 2639-48.

- 988
- 989 Damke, H., D. D. Binns, H. Ueda, S. L. Schmid, and T. Baba. 2001. "Dynamin GTPase Domain
- 990 Mutants Block Endocytic Vesicle Formation at Morphologically Distinct Stages."
- 991 *Molecular Biology of the Cell* 12 (9): 2578–89.
- 992
- 993 De Craene, Johan-Owen, Dimitri L. Bertazzi, Séverine Bär, and Sylvie Friant. 2017.
- 994 "Phosphoinositides, Major Actors in Membrane Trafficking and Lipid Signaling
- 995 Pathways." *International Journal of Molecular Sciences* 18 (3).
- 996 <https://doi.org/10.3390/ijms18030634>.
- 997
- 998 Denk, Winfried, and Heinz Horstmann. 2004. "Serial Block-Face Scanning Electron
- 999 Microscopy to Reconstruct Three-Dimensional Tissue Nanostructure." *PLoS Biology*
- 1000 2 (11): e329. <https://doi.org/10.1371/journal.pbio.0020329>.
- 1001
- 1002 Doherty, Johnna, Mary A. Logan, Ozge E. Tasdemir, and Marc R. Freeman. 2009.
- 1003 "Ensheathing Glia Function as Phagocytes in the Adult Drosophila Brain." *The*
- 1004 *Journal of Neuroscience : The Official Journal of the Society for Neuroscience* 29 (15):
- 1005 4768–81. <https://doi.org/10.1523/JNEUROSCI.5951-08.2009>.
- 1006
- 1007 Dong, Xintong, Oliver W. Liu, Audrey S. Howell, and Kang Shen. 2013. "An Extracellular
- 1008 Adhesion Molecule Complex Patterns Dendritic Branching and Morphogenesis." *Cell*
- 1009 155 (2): 296–307. <https://doi.org/10.1016/j.cell.2013.08.059>.
- 1010
- 1011 D'Souza-Schorey, Crislyn, and Philippe Chavrier. 2006. "ARF Proteins: Roles in Membrane
- 1012 Traffic and Beyond." *Nature Reviews. Molecular Cell Biology* 7 (5): 347–58.
- 1013 <https://doi.org/10.1038/nrm1910>.
- 1014
- 1015 El Sayegh, T. Y., P. D. Arora, K. Ling, C. Laschinger, P. A. Janmey, R. A. Anderson, and C. A.
- 1016 McCulloch. 2007. "Phosphatidylinositol-4,5 Bisphosphate Produced by
- 1017 PIP5K γ Regulates Gelsolin, Actin Assembly, and Adhesion Strength of N-
- 1018 Cadherin Junctions." *Molecular Biology of the Cell* 18 (8): 3026–38.
- 1019 <https://doi.org/10.1091/mbc.e06-12-1159>.
- 1020
- 1021 Ellis, Kathryn, Jennifer Bagwell, and Michel Bagnat. 2013. "Notochord Vacuoles Are
- 1022 Lysosome-Related Organelles That Function in Axis and Spine Morphogenesis." *The*
- 1023 *Journal of Cell Biology* 200 (5): 667–79. <https://doi.org/10.1083/jcb.201212095>.
- 1024
- 1025 Faroni, Alessandro, Luca Franco Castelnovo, Patrizia Procacci, Lucia Caffino, Fabio
- 1026 Fumagalli, Simona Melfi, Giovanna Gambarotta, Bernhard Bettler, Lawrence
- 1027 Wrabetz, and Valerio Magnaghi. 2014. "Deletion of GABA-B Receptor in Schwann
- 1028 Cells Regulates Remak Bundles and Small Nociceptive C-Fibers." *Glia* 62 (4): 548–65.
- 1029 <https://doi.org/10.1002/glia.22625>.
- 1030
- 1031 Gambhir, Alok, Gyöngyi Hangyás-Mihályné, Irina Zaitseva, David S. Cafiso, Jiyao Wang,
- 1032 Diana Murray, Srinivas N. Pentyla, Steven O. Smith, and Stuart McLaughlin. 2004.
- 1033 "Electrostatic Sequestration of PIP2 on Phospholipid Membranes by Basic/Aromatic

- Regions of Proteins." *Biophysical Journal* 86 (4): 2188–2207.
[https://doi.org/10.1016/S0006-3495\(04\)74278-2](https://doi.org/10.1016/S0006-3495(04)74278-2).
- Garrett, Andrew M., Dietmar Schreiner, Mark A. Lobas, and Joshua A. Weiner. 2012. "γ-Protocadherins Control Cortical Dendrite Arborization by Regulating the Activity of a FAK/PKC/MARCKS Signaling Pathway." *Neuron* 74 (2): 269–76.
<https://doi.org/10.1016/j.neuron.2012.01.028>.
- Glaser, M., S. Wanaski, C. A. Buser, V. Boguslavsky, W. Rashidzada, A. Morris, M. Rebecchi, et al. 1996. "Myristoylated Alanine-Rich C Kinase Substrate (MARCKS) Produces Reversible Inhibition of Phospholipase C by Sequestering Phosphatidylinositol 4,5-Bisphosphate in Lateral Domains." *The Journal of Biological Chemistry* 271 (42): 26187–93.
- Gorczyca, David A., Susan Younger, Shan Meltzer, Sung Eun Kim, Li Cheng, Wei Song, Hye Young Lee, Lily Yeh Jan, and Yuh Nung Jan. 2014. "Identification of Ppk26, a DEG/ENAC Channel Functioning with Ppk1 in a Mutually Dependent Manner to Guide Locomotion Behavior in *Drosophila*." *Cell Reports* 9 (4): 1446–58.
<https://doi.org/10.1016/j.celrep.2014.10.034>.
- Grueber, Wesley B, Bing Ye, Adrian W Moore, Lily Y Jan, and Yuh Nung Jan. 2003. "Dendrites of Distinct Classes of *Drosophila* Sensory Neurons Show Different Capacities for Homotypic Repulsion." *Current Biology* 13 (8): 618–26.
- Han, Chun, Lily Yeh Jan, and Yuh-Nung Jan. 2011. "Enhancer-Driven Membrane Markers for Analysis of Nonautonomous Mechanisms Reveal Neuron–Glia Interactions in *Drosophila*." *Proceedings of the National Academy of Sciences* 108 (23): 9673–78.
<https://doi.org/10.1073/pnas.1106386108>.
- Han, Chun, Yuanquan Song, Hui Xiao, Denan Wang, Nathalie C. Franc, Lily Yeh Jan, and Yuh-Nung Jan. 2014. "Epidermal Cells Are the Primary Phagocytes in the Fragmentation and Clearance of Degenerating Dendrites in *Drosophila*." *Neuron* 81 (3): 544–60.
<https://doi.org/10.1016/j.neuron.2013.11.021>.
- Han, Chun, Denan Wang, Peter Soba, Sijun Zhu, Xinhua Lin, Lily Yeh Jan, and Yuh-Nung Jan. 2012. "Integrins Regulate Repulsion-Mediated Dendritic Patterning of *Drosophila* Sensory Neurons by Restricting Dendrites in a 2D Space." *Neuron* 73 (1): 64–78.
<https://doi.org/10.1016/j.neuron.2011.10.036>.
- Hardie, Roger C., Che-Hsiung Liu, Alexander S. Randall, and Sukanya Sengupta. 2015. "In Vivo Tracking of Phosphoinositides in *Drosophila* Photoreceptors." *Journal of Cell Science* 128 (23): 4328–40. <https://doi.org/10.1242/jcs.180364>.
- Helker, Christian S. M., Annika Schuermann, Terhi Karpanen, Dagmar Zeuschner, Heinz-Georg Belting, Markus Affolter, Stefan Schulte-Merker, and Wiebke Herzog. 2013. "The Zebrafish Common Cardinal Veins Develop by a Novel Mechanism: Lumen

- 1080 Ensheathment." *Development* 140 (13): 2776–86.
- 1081 <https://doi.org/10.1242/dev.091876>.
- 1082
- 1083 Honda, A., M. Nogami, T. Yokozeki, M. Yamazaki, H. Nakamura, H. Watanabe, K. Kawamoto,
- 1084 et al. 1999. "Phosphatidylinositol 4-Phosphate 5-Kinase Alpha Is a Downstream
- 1085 Effector of the Small G Protein ARF6 in Membrane Ruffle Formation." *Cell* 99 (5):
- 1086 521–32.
- 1087
- 1088 Jiang, Nan, Hyeon-Jin Kim, Tyler J. Chozinski, Jorge E. Azpurua, Benjamin A. Eaton, Joshua C.
- 1089 Vaughan, and Jay Z. Parrish. 2018. "Super-Resolution Imaging of Drosophila Tissues
- 1090 Using Expansion Microscopy." *Molecular Biology of the Cell*, April, mbcE17100583.
- 1091 <https://doi.org/10.1091/mbc.E17-10-0583>.
- 1092
- 1093 Jiang, Nan, Peter Soba, Edward Parker, Charles C. Kim, and Jay Z. Parrish. 2014. "The
- 1094 MicroRNA Bantam Regulates a Developmental Transition in Epithelial Cells That
- 1095 Restricts Sensory Dendrite Growth." *Development* 141 (13): 2657–68.
- 1096 <https://doi.org/10.1242/dev.107573>.
- 1097
- 1098 Kachur, Torah M., Anjon Audhya, and Dave B. Pilgrim. 2008. "UNC-45 Is Required for NMY-
- 1099 2 Contractile Function in Early Embryonic Polarity Establishment and Germline
- 1100 Cellularization in *C. Elegans*." *Developmental Biology* 314 (2): 287–99.
- 1101 <https://doi.org/10.1016/j.ydbio.2007.11.028>.
- 1102
- 1103 Kawakami, T., M. Ishihara, and M. Mihara. 2001. "Distribution Density of Intraepidermal
- 1104 Nerve Fibers in Normal Human Skin." *The Journal of Dermatology* 28 (2): 63–70.
- 1105
- 1106 Kim, Michelle E, Brikha R Shrestha, Richard Blazeski, Carol A Mason, and Wesley B Grueber.
- 1107 2012. "Integrins Establish Dendrite-Substrate Relationships That Promote Dendritic
- 1108 Self-Avoidance and Patterning in Drosophila Sensory Neurons." *Neuron* 73 (1): 79–
- 1109 91. <https://doi.org/10.1016/j.neuron.2011.10.033>.
- 1110
- 1111 Koizumi, Schuichi, Kayoko Fujishita, Kaori Inoue, Yukari Shigemoto-Mogami, Makoto
- 1112 Tsuda, and Kazuhide Inoue. 2004. "Ca²⁺ Waves in Keratinocytes Are Transmitted to
- 1113 Sensory Neurons: The Involvement of Extracellular ATP and P2Y₂ Receptor
- 1114 Activation." *The Biochemical Journal* 380 (Pt 2): 329–38.
- 1115 <https://doi.org/10.1042/BJ20031089>.
- 1116
- 1117 Kwan, Kristen M., Esther Fujimoto, Clemens Grabher, Benjamin D. Mangum, Melissa E.
- 1118 Hardy, Douglas S. Campbell, John M. Parant, H. Joseph Yost, John P. Kanki, and Chi-
- 1119 Bin Chien. 2007. "The Tol2kit: A Multisite Gateway-Based Construction Kit for Tol2
- 1120 Transposon Transgenesis Constructs." *Developmental Dynamics* 236 (11): 3088–99.
- 1121 <https://doi.org/10.1002/dvdy.21343>.
- 1122
- 1123 Kwiatkowska, Katarzyna. 2010. "One Lipid, Multiple Functions: How Various Pools of
- 1124 PI(4,5)P₂ Are Created in the Plasma Membrane." *Cellular and Molecular Life*
- 1125 *Sciences: CMLS* 67 (23): 3927–46. <https://doi.org/10.1007/s00018-010-0432-5>.

- 1126
- 1127 Liang, Xing, Xintong Dong, Donald G. Moerman, Kang Shen, and Xiangming Wang. 2015.
- 1128 "Sarcomeres Pattern Proprioceptive Sensory Dendritic Endings through UNC-
- 1129 52/Perlecan in *C. Elegans*." *Developmental Cell* 33 (4): 388–400.
- 1130 <https://doi.org/10.1016/j.devcel.2015.03.010>.
- 1131
- 1132 Ling, Kun, Renee L. Doughman, Ari J. Firestone, Matthew W. Bunce, and Richard A.
- 1133 Anderson. 2002. "Type I Gamma Phosphatidylinositol Phosphate Kinase Targets and
- 1134 Regulates Focal Adhesions." *Nature* 420 (6911): 89–93.
- 1135 <https://doi.org/10.1038/nature01082>.
- 1136
- 1137 Liu, Yongdan, Xueli Fan, Yafen Wei, Zhongyuan Piao, and Xinmei Jiang. 2014.
- 1138 "Intraepidermal Nerve Fiber Density of Healthy Human." *Neurological Research* 36
- 1139 (10): 911–14. <https://doi.org/10.1179/1743132814Y.0000000377>.
- 1140
- 1141 Loewenstein, W. R., and R. Skalak. 1966. "Mechanical Transmission in a Pacinian Corpuscle.
- 1142 An Analysis and a Theory." *The Journal of Physiology* 182 (2): 346–78.
- 1143
- 1144 Longair, Mark H., Dean A. Baker, and J. Douglas Armstrong. 2011. "Simple Neurite Tracer:
- 1145 Open Source Software for Reconstruction, Visualization and Analysis of Neuronal
- 1146 Processes." *Bioinformatics* 27 (17): 2453–54.
- 1147 <https://doi.org/10.1093/bioinformatics/btr390>.
- 1148
- 1149 Maksimovic, Srdjan, Yoshichika Baba, and Ellen A. Lumpkin. 2013. "Neurotransmitters and
- 1150 Synaptic Components in the Merkel Cell-Neurite Complex, a Gentle-Touch
- 1151 Receptor." *Annals of the New York Academy of Sciences* 1279 (March): 13–21.
- 1152 <https://doi.org/10.1111/nyas.12057>.
- 1153
- 1154 Maksimovic, Srdjan, Masashi Nakatani, Yoshichika Baba, Aislyn M. Nelson, Kara L. Marshall,
- 1155 Scott A. Wellnitz, Pervez Firozi, et al. 2014. "Epidermal Merkel Cells Are
- 1156 Mechanosensory Cells That Tune Mammalian Touch Receptors." *Nature* 509 (7502):
- 1157 617–21. <https://doi.org/10.1038/nature13250>.
- 1158
- 1159 McLaughlin, Stuart, and Diana Murray. 2005. "Plasma Membrane Phosphoinositide
- 1160 Organization by Protein Electrostatics." *Nature* 438 (7068): 605–11.
- 1161 <https://doi.org/10.1038/nature04398>.
- 1162
- 1163 Michailov, Galin V., Michael W. Sereda, Bastian G. Brinkmann, Tobias M. Fischer, Bernhard
- 1164 Haug, Carmen Birchmeier, Lorna Role, Cary Lai, Markus H. Schwab, and Klaus-Armin
- 1165 Nave. 2004. "Axonal Neuregulin-1 Regulates Myelin Sheath Thickness." *Science* 304
- 1166 (5671): 700–703. <https://doi.org/10.1126/science.1095862>.
- 1167
- 1168 Mihara, M., K. Hashimoto, K. Ueda, and M. Kumakiri. 1979. "The Specialized Junctions
- 1169 between Merkel Cell and Neurite: An Electron Microscopic Study." *The Journal of*
- 1170 *Investigative Dermatology* 73 (5): 325–34.
- 1171

- 1172 Moehring, Francie, Ashley M. Cowie, Anthony D. Menzel, Andy D. Weyer, Michael
- 1173 Grzybowski, Thiago Arzua, Aron M. Geurts, Oleg Palygin, and Cheryl L. Stucky. 2018.
- 1174 "Keratinocytes Mediate Innocuous and Noxious Touch via ATP-P2X4 Signaling."
- 1175 *ELife* 7. <https://doi.org/10.7554/eLife.31684>.
- 1176
- 1177 Munger, B. L. 1965. "The Intraepidermal Innervation of the Snout Skin of the Opossum. A
- 1178 Light and Electron Microscope Study, with Observations on the Nature of Merkel's
- 1179 Tastzellen." *The Journal of Cell Biology* 26 (1): 79–97.
- 1180
- 1181 Myat, M. M., S. Anderson, L. A. Allen, and A. Aderem. 1997. "MARCKS Regulates Membrane
- 1182 Ruffling and Cell Spreading." *Current Biology* 7 (8): 611–14.
- 1183
- 1184 Nguyen, Minh Q., Youmei Wu, Lauren S. Bonilla, Lars J. von Buchholtz, and Nicholas J. P.
- 1185 Ryba. 2017. "Diversity amongst Trigeminal Neurons Revealed by High Throughput
- 1186 Single Cell Sequencing." *PloS One* 12 (9): e0185543.
- 1187 <https://doi.org/10.1371/journal.pone.0185543>.
- 1188
- 1189 O'Brien, Georgeann S., Seanna M. Martin, Christian Söllner, Gavin J. Wright, Catherina G.
- 1190 Becker, Carlos Portera-Cailliau, and Alvaro Sagasti. 2009. "Developmentally
- 1191 Regulated Impediments to Skin Reinnervation by Injured Peripheral Sensory Axon
- 1192 Terminals." *Current Biology* 19 (24): 2086–90.
- 1193 <https://doi.org/10.1016/j.cub.2009.10.051>.
- 1194
- 1195 O'Brien, Georgeann S., Sandra Rieger, Seanna M. Martin, Ann M. Cavanaugh, Carlos Portera-
- 1196 Cailliau, and Alvaro Sagasti. 2009. "Two-Photon Axotomy and Time-Lapse Confocal
- 1197 Imaging in Live Zebrafish Embryos." *Journal of Visualized Experiments: JoVE*, no. 24.
- 1198 <https://doi.org/10.3791/1129>.
- 1199
- 1200 O'Brien, Georgeann S., Sandra Rieger, Fang Wang, Gromoslaw A. Smolen, Robert E.
- 1201 Gonzalez, JoAnn Buchanan, and Alvaro Sagasti. 2012. "Coordinate Development of
- 1202 Skin Cells and Cutaneous Sensory Axons in Zebrafish." *The Journal of Comparative*
- 1203 *Neurology* 520 (4): 816–31. <https://doi.org/10.1002/cne.22791>.
- 1204
- 1205 Orita, Sumihisa, Kenneth Henry, Elisabetta Mantuano, Kazuyo Yamauchi, Alice De Corato,
- 1206 Tetsuhiro Ishikawa, M. Laura Feltri, et al. 2013. "Schwann Cell LRP1 Regulates
- 1207 Remak Bundle Ultrastructure and Axonal Interactions to Prevent Neuropathic Pain."
- 1208 *The Journal of Neuroscience: The Official Journal of the Society for Neuroscience* 33
- 1209 (13): 5590–5602. <https://doi.org/10.1523/JNEUROSCI.3342-12.2013>.
- 1210
- 1211 Owens, David M., and Ellen A. Lumpkin. 2014. "Diversification and Specialization of Touch
- 1212 Receptors in Skin." *Cold Spring Harbor Perspectives in Medicine* 4 (6).
- 1213 <https://doi.org/10.1101/cshperspect.a013656>.
- 1214
- 1215 Pang, Zixuan, Takashi Sakamoto, Vinod Tiwari, Yu-Shin Kim, Fei Yang, Xinzhong Dong, Ali
- 1216 D. Güler, Yun Guan, and Michael J. Caterina. 2015. "Selective Keratinocyte

- 1217 Stimulation Is Sufficient to Evoke Nociception in Mice." *Pain* 156 (4): 656–65.
- 1218 <https://doi.org/10.1097/j.pain.000000000000092>.
- 1219
- 1220 Parrish, Jay Z, Peizhang Xu, Charles C Kim, Lily Yeh Jan, and Yuh Nung Jan. 2009. "The
- 1221 MicroRNA Bantam Functions in Epithelial Cells to Regulate Scaling Growth of
- 1222 Dendrite Arbors in Drosophila Sensory Neurons." *Neuron* 63 (6): 788–802.
- 1223 <https://doi.org/10.1016/j.neuron.2009.08.006>.
- 1224
- 1225 Peier, Andrea M., Alison J. Reeve, David A. Andersson, Aziz Moqrich, Taryn J. Earley, Anne C.
- 1226 Hergarden, Gina M. Story, et al. 2002. "A Heat-Sensitive TRP Channel Expressed in
- 1227 Keratinocytes." *Science* 296 (5575): 2046–49.
- 1228 <https://doi.org/10.1126/science.1073140>.
- 1229
- 1230 Raphael, Alya R., Julie R. Perlin, and William S. Talbot. 2010. "Schwann Cells Reposition a
- 1231 Peripheral Nerve to Isolate It from Postembryonic Remodeling of Its Targets."
- 1232 *Development* 137 (21): 3643–49. <https://doi.org/10.1242/dev.057521>.
- 1233
- 1234 Rasmussen, Jeffrey P., Georgeann S. Sack, Seanna M. Martin, and Alvaro Sagasti. 2015.
- 1235 "Vertebrate Epidermal Cells Are Broad-Specificity Phagocytes That Clear Sensory
- 1236 Axon Debris." *The Journal of Neuroscience: The Official Journal of the Society for*
- 1237 *Neuroscience* 35 (2): 559–70. <https://doi.org/10.1523/JNEUROSCI.3613-14.2015>.
- 1238
- 1239 Rasmussen, Jeffrey P., Nhat-Thi Vo, and Alvaro Sagasti. 2018. "Fish Scales Dictate the
- 1240 Pattern of Adult Skin Innervation and Vascularization." *Developmental Cell* 46 (3):
- 1241 344–359.e4. <https://doi.org/10.1016/j.devcel.2018.06.019>.
- 1242
- 1243 Raucher, D., T. Stauffer, W. Chen, K. Shen, S. Guo, J. D. York, M. P. Sheetz, and T. Meyer. 2000.
- 1244 "Phosphatidylinositol 4,5-Bisphosphate Functions as a Second Messenger That
- 1245 Regulates Cytoskeleton-Plasma Membrane Adhesion." *Cell* 100 (2): 221–28.
- 1246
- 1247 Risse, Benjamin, Silke Thomas, Nils Otto, Tim Löpmeier, Dimitar Valkov, Xiaoyi Jiang, and
- 1248 Christian Klämbt. 2013. "FIM, a Novel FTIR-Based Imaging Method for High
- 1249 Throughput Locomotion Analysis." *PloS One* 8 (1): e53963.
- 1250 <https://doi.org/10.1371/journal.pone.0053963>.
- 1251
- 1252 Sakai, T., J. Kasuya, T. Kitamoto, and T. Aigaki. 2009. "The Drosophila TRPA Channel,
- 1253 Painless, Regulates Sexual Receptivity in Virgin Females." *Genes, Brain, and Behavior*
- 1254 8 (5): 546–57. <https://doi.org/10.1111/j.1601-183X.2009.00503.x>.
- 1255
- 1256 Salzberg, Yehuda, Carlos A Díaz-Balzac, Nelson J Ramirez-Suarez, Matthew Attreed, Eillen
- 1257 Tecle, Muriel Desbois, Zaven Kaprielian, and Hannes E Bülow. 2013. "Skin-Derived
- 1258 Cues Control Arborization of Sensory Dendrites in Caenorhabditis Elegans." *Cell* 155
- 1259 (2): 308–20. <https://doi.org/10.1016/j.cell.2013.08.058>.
- 1260
- 1261 Schindelin, Johannes, Ignacio Arganda-Carreras, Erwin Frise, Verena Kaynig, Mark Longair,
- 1262 Tobias Pietzsch, Stephan Preibisch, et al. 2012. "Fiji: An Open-Source Platform for

- Biological-Image Analysis." *Nature Methods* 9 (7): 676–82.
<https://doi.org/10.1038/nmeth.2019>.
- Scott, Cameron C., Wendy Dobson, Roberto J. Botelho, Natasha Coady-Osberg, Philippe Chavrier, David A. Knecht, Colin Heath, Philip Stahl, and Sergio Grinstein. 2005. "Phosphatidylinositol-4,5-Bisphosphate Hydrolysis Directs Actin Remodeling during Phagocytosis." *The Journal of Cell Biology* 169 (1): 139–49.
<https://doi.org/10.1083/jcb.200412162>.
- Song, Wei, Maika Onishi, Lily Yeh Jan, and Yuh Nung Jan. 2007. "Peripheral Multidendritic Sensory Neurons Are Necessary for Rhythmic Locomotion Behavior in *Drosophila* Larvae." *Proceedings of the National Academy of Sciences of the United States of America* 104 (12): 5199–5204. <https://doi.org/10.1073/pnas.0700895104>.
- Sugimura, Kaoru, Misato Yamamoto, Ryusuke Niwa, Daisuke Satoh, Satoshi Goto, Misako Taniguchi, Shigeo Hayashi, and Tadashi Uemura. 2003. "Distinct Developmental Modes and Lesion-Induced Reactions of Dendrites of Two Classes of *Drosophila* Sensory Neurons." *The Journal of Neuroscience: The Official Journal of the Society for Neuroscience* 23 (9): 3752–60.
- Sun, Yue, Narendra Thapa, Andrew C. Hedman, and Richard A. Anderson. 2013. "Phosphatidylinositol 4,5-Bisphosphate: Targeted Production and Signaling." *BioEssays: News and Reviews in Molecular, Cellular and Developmental Biology* 35 (6): 513–22. <https://doi.org/10.1002/bies.201200171>.
- Suster, Maximiliano L., Gembu Abe, Anders Schouw, and Koichi Kawakami. 2011. "Transposon-Mediated BAC Transgenesis in Zebrafish." *Nature Protocols* 6 (12): 1998–2021. <https://doi.org/10.1038/nprot.2011.416>.
- Tenenbaum, Conrad M., Mala Misra, Rebecca A. Alizzi, and Elizabeth R. Gavis. 2017. "Enclosure of Dendrites by Epidermal Cells Restricts Branching and Permits Coordinated Development of Spatially Overlapping Sensory Neurons." *Cell Reports* 20 (13): 3043–56. <https://doi.org/10.1016/j.celrep.2017.09.001>.
- Trinh, Le A., Tatiana Hochgreb, Matthew Graham, David Wu, Frederique Ruf-Zamojski, Chathurani S. Jayasena, Ankur Saxena, et al. 2011. "A Versatile Gene Trap to Visualize and Interrogate the Function of the Vertebrate Proteome." *Genes & Development* 25 (21): 2306–20. <https://doi.org/10.1101/gad.174037.111>.
- Üçeyler, Nurcan, Daniel Zeller, Ann-Kathrin Kahn, Susanne Kewenig, Sarah Kittel-Schneider, Annina Schmid, Jordi Casanova-Molla, Karlheinz Reiners, and Claudia Sommer. 2013. "Small Fibre Pathology in Patients with Fibromyalgia Syndrome." *Brain: A Journal of Neurology* 136 (Pt 6): 1857–67.
<https://doi.org/10.1093/brain/awt053>.

- 1308 Usoskin, Dmitry, Alessandro Furlan, Saiful Islam, Hind Abdo, Peter Lönnerberg, Daohua
- 1309 Lou, Jens Hjerling-Leffler, et al. 2015. "Unbiased Classification of Sensory Neuron
- 1310 Types by Large-Scale Single-Cell RNA Sequencing." *Nature Neuroscience* 18 (1):
- 1311 145–53. <https://doi.org/10.1038/nn.3881>.
- 1312
- 1313 Várnai, P., and T. Balla. 1998. "Visualization of Phosphoinositides That Bind Pleckstrin
- 1314 Homology Domains: Calcium- and Agonist-Induced Dynamic Changes and
- 1315 Relationship to Myo-[3H]Inositol-Labeled Phosphoinositide Pools." *The Journal of*
- 1316 *Cell Biology* 143 (2): 501–10.
- 1317
- 1318 Verstreken, Patrik, Tomoko Ohyama, Claire Haueter, Ron L. P. Habets, Yong Q. Lin, Laura E.
- 1319 Swan, Cindy V. Ly, Koen J. T. Venken, Pietro De Camilli, and Hugo J. Bellen. 2009.
- 1320 "Tweek, an Evolutionarily Conserved Protein, Is Required for Synaptic Vesicle
- 1321 Recycling." *Neuron* 63 (2): 203–15. <https://doi.org/10.1016/j.neuron.2009.06.017>.
- 1322
- 1323 Weis, J., I. Katona, G. Müller-Newen, C. Sommer, G. Necula, C. Hendrich, A. C. Ludolph, and
- 1324 A.-D. Sperfeld. 2011. "Small-Fiber Neuropathy in Patients with ALS." *Neurology* 76
- 1325 (23): 2024–29. <https://doi.org/10.1212/WNL.0b013e31821e553a>.
- 1326
- 1327 Whitear, M., and R. Moate. 1998. "Cellular Diversity in the Epidermis of Raja Clavata
- 1328 (Chondrichthyes)." *Journal of Zoology* 246 (3): 275–85.
- 1329 <https://doi.org/10.1111/j.1469-7998.1998.tb00158.x>.
- 1330
- 1331 Woo, Seung-Hyun, Sanjeev Ranade, Andy D. Weyer, Adrienne E. Dubin, Yoshichika Baba,
- 1332 Zhaozhu Qiu, Matt Petrus, et al. 2014. "Piezo2 Is Required for Merkel-Cell
- 1333 Mechanotransduction." *Nature* 509 (7502): 622–26.
- 1334 <https://doi.org/10.1038/nature13251>.
- 1335
- 1336 Woolf, C. J., A. Allchorne, B. Safieh-Garabedian, and S. Poole. 1997. "Cytokines, Nerve
- 1337 Growth Factor and Inflammatory Hyperalgesia: The Contribution of Tumour
- 1338 Necrosis Factor Alpha." *British Journal of Pharmacology* 121 (3): 417–24.
- 1339 <https://doi.org/10.1038/sj.bjp.0701148>.
- 1340
- 1341 Xiong, Xunhao, Qingwen Xu, Yan Huang, Raman Deep Singh, Richard Anderson, Edward
- 1342 Leof, Jinghua Hu, and Kun Ling. 2012. "An Association between Type Iy PI4P 5-
- 1343 Kinase and Exo70 Directs E-Cadherin Clustering and Epithelial Polarization."
- 1344 *Molecular Biology of the Cell* 23 (1): 87–98. [https://doi.org/10.1091/mbc.E11-05-](https://doi.org/10.1091/mbc.E11-05-0449)
- 1345 [0449](https://doi.org/10.1091/mbc.E11-05-0449).
- 1346
- 1347 Xu, Haoxing, Markus Delling, Janice C. Jun, and David E. Clapham. 2006. "Oregano, Thyme
- 1348 and Clove-Derived Flavors and Skin Sensitizers Activate Specific TRP Channels."
- 1349 *Nature Neuroscience* 9 (5): 628–35. <https://doi.org/10.1038/nn1692>.
- 1350
- 1351 Yin, Helen L., and Paul A. Janmey. 2003. "Phosphoinositide Regulation of the Actin
- 1352 Cytoskeleton." *Annual Review of Physiology* 65: 761–89.
- 1353 <https://doi.org/10.1146/annurev.physiol.65.092101.142517>.

1354
 1355 Zhong, Lixian, Richard Y. Hwang, and W. Daniel Tracey. 2010. "Pickpocket Is a DEG/ENaC
 1356 Protein Required for Mechanical Nociception in Drosophila Larvae." *Current Biology*
 1357 20 (5): 429–34. <https://doi.org/10.1016/j.cub.2009.12.057>.
 1358
 1359 Zimmerman, Amanda, Ling Bai, and David D. Ginty. 2014. "The Gentle Touch Receptors of
 1360 Mammalian Skin." *Science (New York, N.Y.)* 346 (6212): 950–54.
 1361 <https://doi.org/10.1126/science.1254229>.
 1362

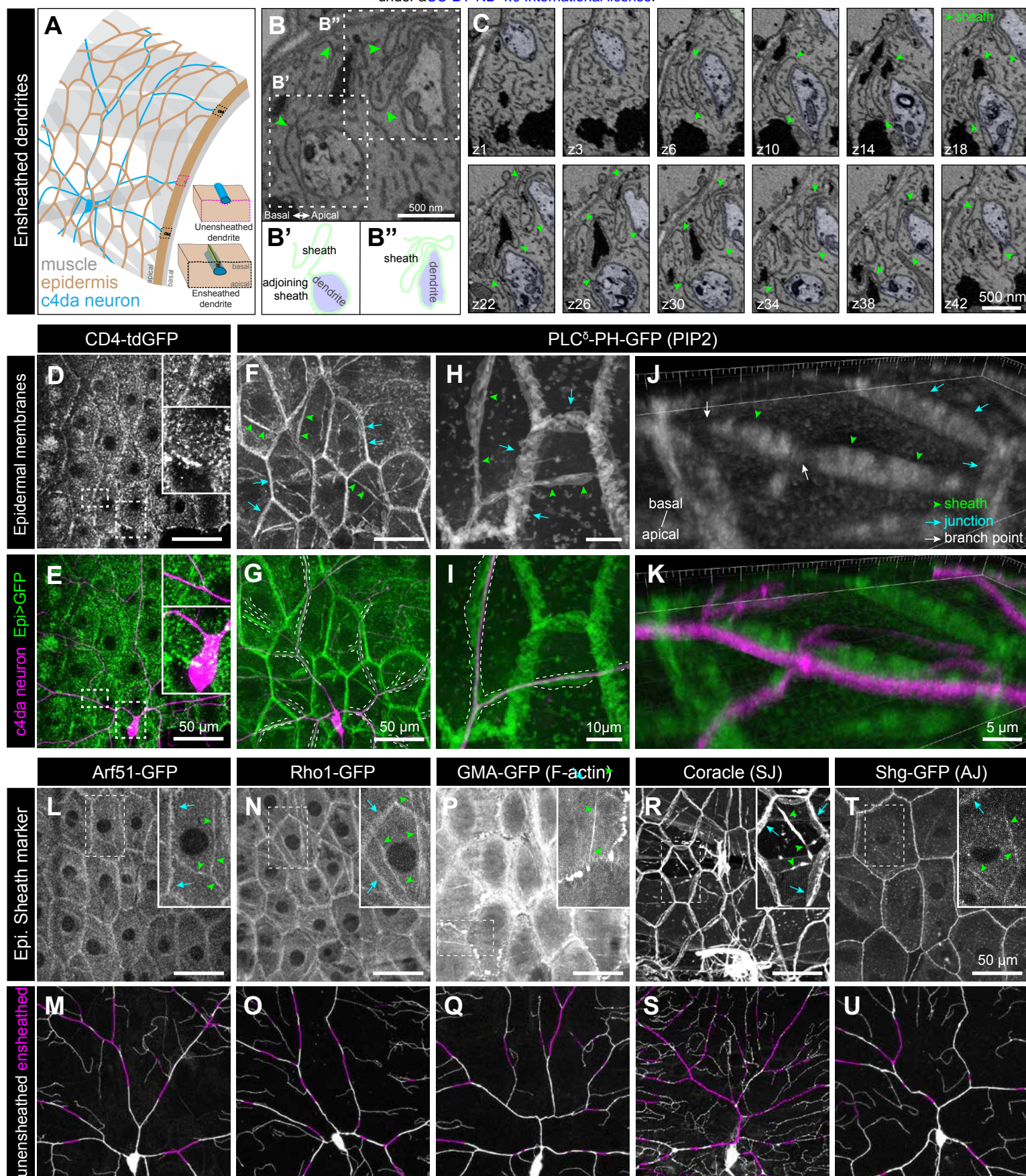


Figure 1. Epidermal PIP2 accumulation marks sites of dendrite ensheathment. (A) Schematic view of *Drosophila* larval body wall. Ensheathed and unensheathed dendrites are depicted in cross-section. (legend continued on next page)

Figure 1. Epidermal PIP2 accumulation marks sites of dendrite ensheathment. (B-C) SBF-SEM analysis of epidermal dendrite ensheathment. (B' and B'') Traces of da neuron dendrites and epidermal sheaths in cross-section. (C) Serial sections showing epidermal ensheathment (arrowheads mark sheaths) of da neuron dendrites (shaded green). The dendrite present in sections z1-z38 branches inside an epidermal sheath. See also Figure 1 – movie supplement 1. (D-E) Assay for markers of dendrite ensheathment. GFP-tagged markers were specifically expressed in the epidermis (A58-Gal4, Cha-Gal80) in larvae expressing the c4da-specific marker ppk-CD4-tdTomato. Maximum intensity projection of membrane-targeted CD4-tdGFP (D) and c4da dendrites (E) are shown. Insets show magnified views of c4da dendrites (top) and c4da soma (bottom). (F-K) Epidermal PLC δ -PH-GFP labels sites of dendrite ensheathment. Maximum intensity projections of epidermal PLC δ -PH-GFP (F, H, J) and overlay showing PLC δ -PH-GFP signal in green and ppk-CD4-tdTomato in magenta to label c4da dendrites (G, I, K). Hatched lines mark sheaths. (F-I) XY projections of live confocal images. (J-K) Expansion microscopy image showing epithelial PIP2 distribution at sites of c4da dendrite contact. Image shows a side view of a single epithelial cell and ensheathed c4da dendrites oriented along the apical-basal axis (apical, top). Note the discontinuities in the epithelial sheath at the dendrite branch point and at epithelial intracellular junctions (arrowheads). Scale bars have been divided by the measured expansion factor of $\sim 4\times$ and therefore refers to pre-expansion dimensions. (L-U) Epidermal sheath markers. Maximum intensity projections show the distribution of the indicated GFP reporters in the epidermis of 120 h AEL larvae and composites show portions of c4da dendrite arbors (shaded purple) wrapped by sheaths labeled by the GFP reporters. Experimental genotypes of are available in Supplemental Table 2.

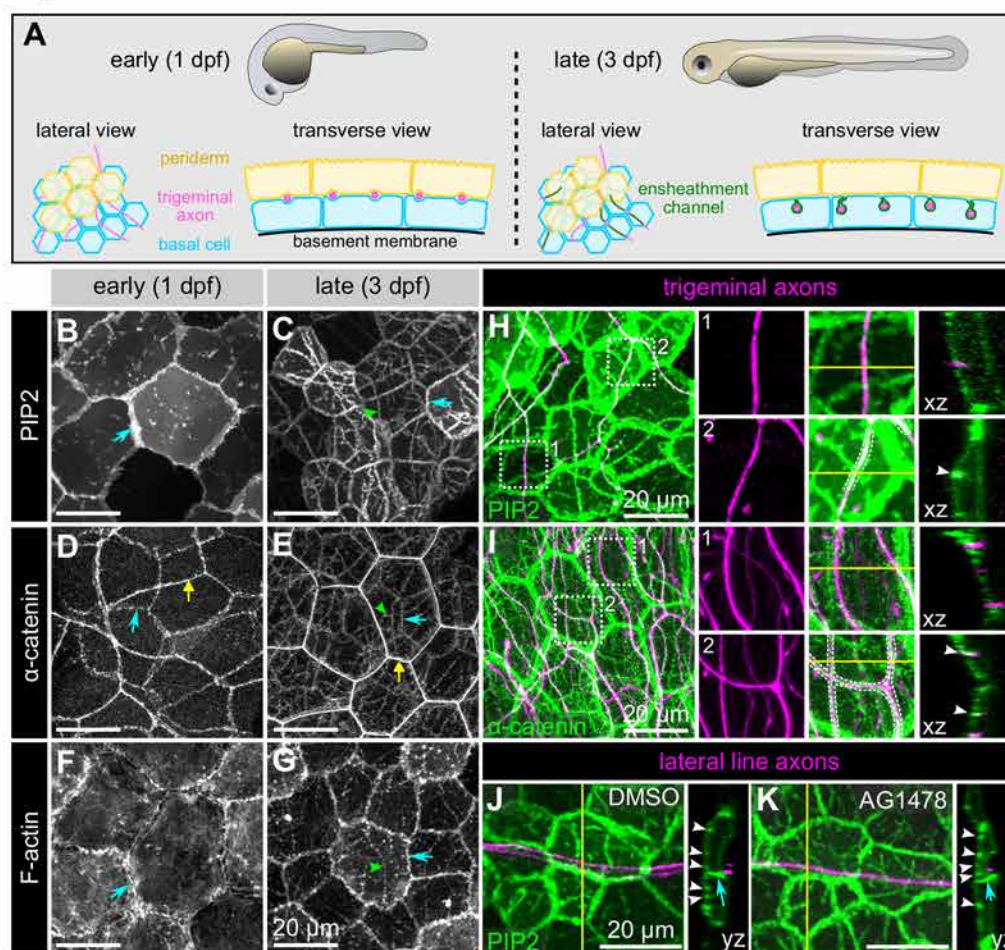


Figure 2. Molecular markers of epidermal sheaths in larval zebrafish. Schematic of the bilayered larval zebrafish epidermis at the indicated stages based on the ultrastructural analysis (O'Brien et al. 2012). (B-G) Maximum intensity projections of confocal z-stacks showing lateral views through the epidermis at 24 hpf (B,D,F) or 72 hpf (C,E,G). Fluorescent reporters for PIP2 (B-C), α -catenin (D-E) and F-actin (F-G) are shown. Note the appearance of linear domains of each reporter through the apical basal cell membrane (green arrowheads) at the later time-point. Cyan arrows indicate basal lateral cell borders. Yellow arrows indicate periderm lateral cell borders. (H,I) Dual-labelling of epidermal sheaths and trigeminal sensory neurons. tdTomato-labeled trigeminal sensory neurons (magenta) together with the PIP2 reporter GFP-PH-PLC in basal cells at 46 hpf (H) or α -catenin-Citrine in both periderm and basal cells (I) at 73 hpf. White dashed lines and arrowheads indicate examples of ensheathment channels containing labeled axons. Yellow lines indicate planes of orthogonal sections. (J,K) tdTomato-labeled posterior lateral line axons (magenta) labeled by transient injection of a *neurod:mTangerine* plasmid are shown together with GFP-PH-PLC signal in basal cells (green) at 78 hpf in either DMSO- or AG1478-treated embryos. AG1478 treatment prevents the repositioning of the posterior lateral line nerve below the epidermis (Raphael, Perlin, and Talbot 2010), resulting in the indentation of basal cell basal cell membranes, but did not trigger the accumulation of the PIP2 reporter GFP-PH-PLC. Arrowheads indicate ensheathment channels along the apical surface of basal cells. Blue arrows indicate basal cell lateral borders. Yellow lines indicate planes of orthogonal sections.

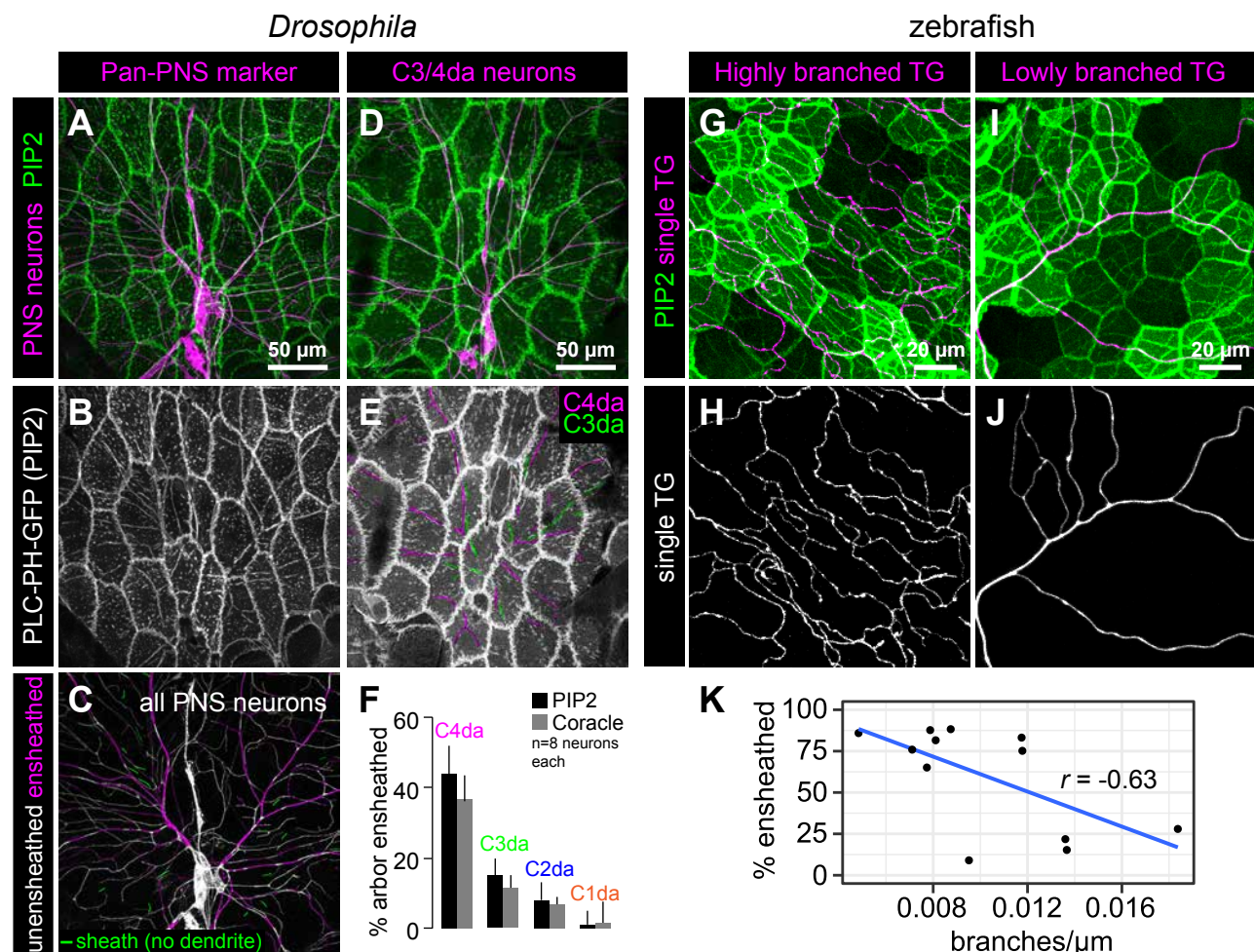


Figure 3. Epithelial sheaths form adjacent to somatosensory neurons in a modality-specific manner. (A-C) Dual-labelling of epithelial sheaths and all somatosensory neurons. Maximum projections of confocal stacks show (A) mRFP-labeled sensory neurons (magenta) together with epidermal PLC δ -PH-GFP signal (green) or (B) epidermal PLC δ -PH-GFP signal on its own. (C) PLC δ -PH-GFP-positive sheaths are pseudocolored with dendrite-associated sheaths shaded in magenta and sheaths without apposed dendrites shaded in green. (D-E) Dual-labeling of epithelial sheaths and c3da/c4da sensory neurons. (D) tdTomato-labeled c3da and c4da neurons (magenta) are shown together with epidermal PLC δ -PH-GFP signal (green). (E) Image showing epidermal PLC δ -PH-GFP signal with c3da-containing sheaths shaded green and c4da-containing sheaths shaded magenta. (F) Histogram depicting mean and standard deviation values for the portion of the dendrite arbor of different classes of da neurons ensheathed by the epidermis using PLC δ -PH-GFP or coracle immunostaining as a marker for ensheathment. (G-K) The extent of ensheathment was inversely correlated with trigeminal (TG) axon complexity in zebrafish. Examples of single TG neurons labeled by transient injection of *Tg(isl1[ss]:L-EXA-VP16,LEXAop:tdTomato)* with high (G,H) or low (I,J) branch density. (K) Scatterplot of axon branches versus percent of axon length ensheathed from tracings of 12 individual TG neurons. Note the inverse linear regression (blue line).



Figure 4. Somatosensory neurons are ne sheaths. (*legend continued on next page*)

Figure 4. Somatosensory neurons are necessary for formation and maintenance of epidermal sheaths. (A-G) Time-course of sheath formation. Maximum intensity projections show dual labeling of sheaths by epidermal PLC δ -PH-GFP and the c4da-specific marker ppk-CD4-tdTomato (A, D) or PLC δ -PH-GFP signal alone (B, E) at 72 and 120 h AEL. (C, F) Composites show portions of c4da dendrite arbors (shaded purple) wrapped by sheaths labeled by PLC δ -PH-GFP. (G) Plots show mean and standard deviation values for the proportion of c4da dendrite arbors wrapped by PLC δ -PH-GFP or coracle-positive sheaths. See also Figure 4 – figure supplement 2 for images of coracle labeling of sheaths at 72 and 120 h AEL. (H) Once formed, sheaths persist. Plot shows sheath dynamics; the proportion of sheaths from 8 neurons that grew, retracted or were stable over a 24 h time-lapse is shown. See also Figure 4 – figure supplement 1 for time-lapse images. (I-K) Epidermal sheath formation following genetic ablation of c4da neurons. Maximum intensity projections show dual labeling of anti-cora staining to label sheaths and anti-HRP staining to label PNS neurons (I) and the individual markers alone (J, K) at 120 h AEL for a larva expressing the pro-apoptotic gene reaper (rpr) specifically in c4da neurons under control of ppk-Gal4. (L-N) Epidermal sheath formation following laser ablation of larval c2da, c3da, and c4da neurons. Images show dual labeling of epidermal sheaths with anti-cora staining and sensory neurons with anti-HRP staining (L) and the individual markers alone (M, N) at 120 h AEL in a hemisegment in which c2da, c3da, and c4da were ablated with a focused laser beam at 72 h AEL. (O-T) Somatosensory dendrites are required for sheath maintenance. Maximum projections of confocal stacks show time-lapse images of da neurons labeled with membrane-targeted mRFP (O) and epidermal sheaths (P) immediately prior to c4da dendrite severing at 108 h AEL and 12 h post-severing at 120 h AEL (R, S). White dashed lines outline the anterior-dorsal portions of the c4da arbor that are ensheathed prior to severing and the location those sheaths would occupy if they persisted post-severing. (Q, T) Traces depict unensheathed c4da dendrites in black and ensheathed c4da dendrites in green, the arrow marks the site of dendrite severing, and the gray box marks the quadrant in which c4da dendrites and associated epidermal sheaths are lost post-severing. (U-Z) Epidermal sheath formation in zebrafish injected of a morpholino targeting neurog1 to prevent somatosensory neuron development. Maximum intensity projections of confocal z-stacks showing lateral views through the zebrafish epidermis at 72 hpf. Note the lack of ensheathment channels (green arrowheads) in neurog1(MO)-injected embryos. Yellow and cyan arrows indicate the lateral cell membranes of periderm and basal cells, respectively. (AA) Somatosensory axons are required for sheath maintenance in zebrafish.

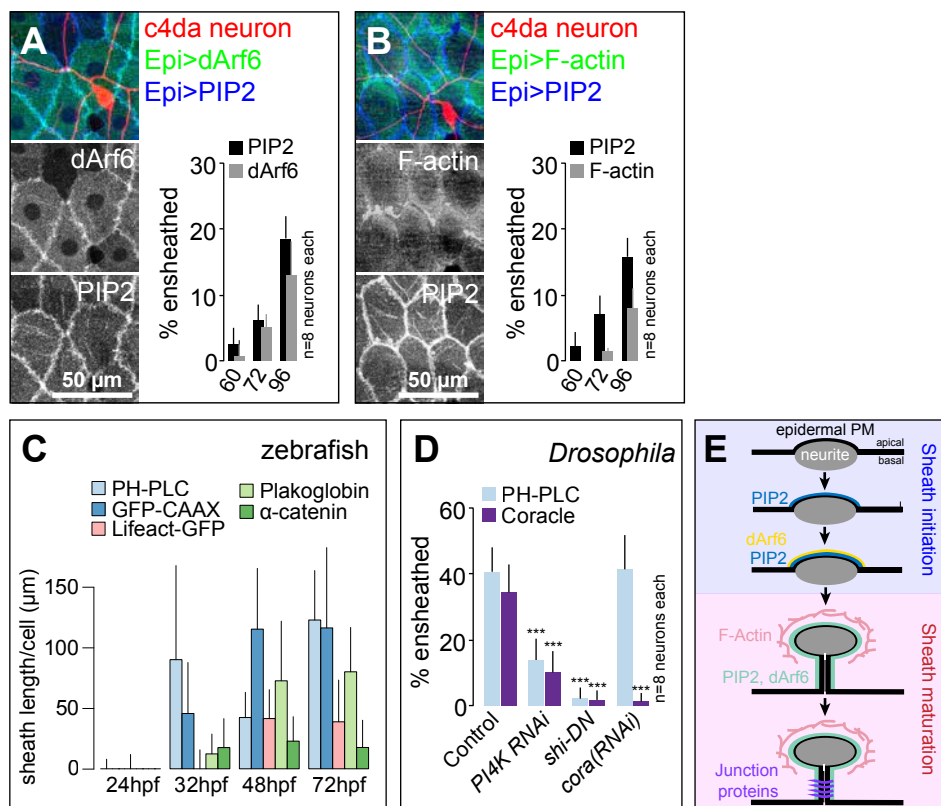


Figure 5. Sequence of events in sheath assembly. (A-B) Time of arrival of PIP2 and other sheath markers. Images show dual labeling of sheaths by PLC δ -PH-Cerulean and dArf6-GFP (A) or GMA-GFP to label F-actin (B) in larvae additionally expressing the c4da-specific marker ppk-CD4-tdTomato. Plots show the mean and standard deviation values for the proportion of c4da dendrite arbors ensheathed by structures labeled by the indicated markers at the indicated times. All sheath structures labeled by dArf6-GFP and GMA-GFP were labeled by PLC δ -PH-Cerulean. (C) Timing of accumulation of ensheathment channel markers in the zebrafish epidermis. (D) Epistatic relationship between markers. The indicated RNAi transgenes were expressed in the epidermis and effects on ensheathment were assessed (see Figure 5 – figure supplement 2 for accompanying images). Plots show mean and standard deviation values for the proportion of c4da dendrite arbors wrapped by PLC δ -PH-GFP or coracle-positive sheaths. n = 8 neurons each; ***P<0.001 relative to control; one way ANOVA with post-hoc Dunnett's test.

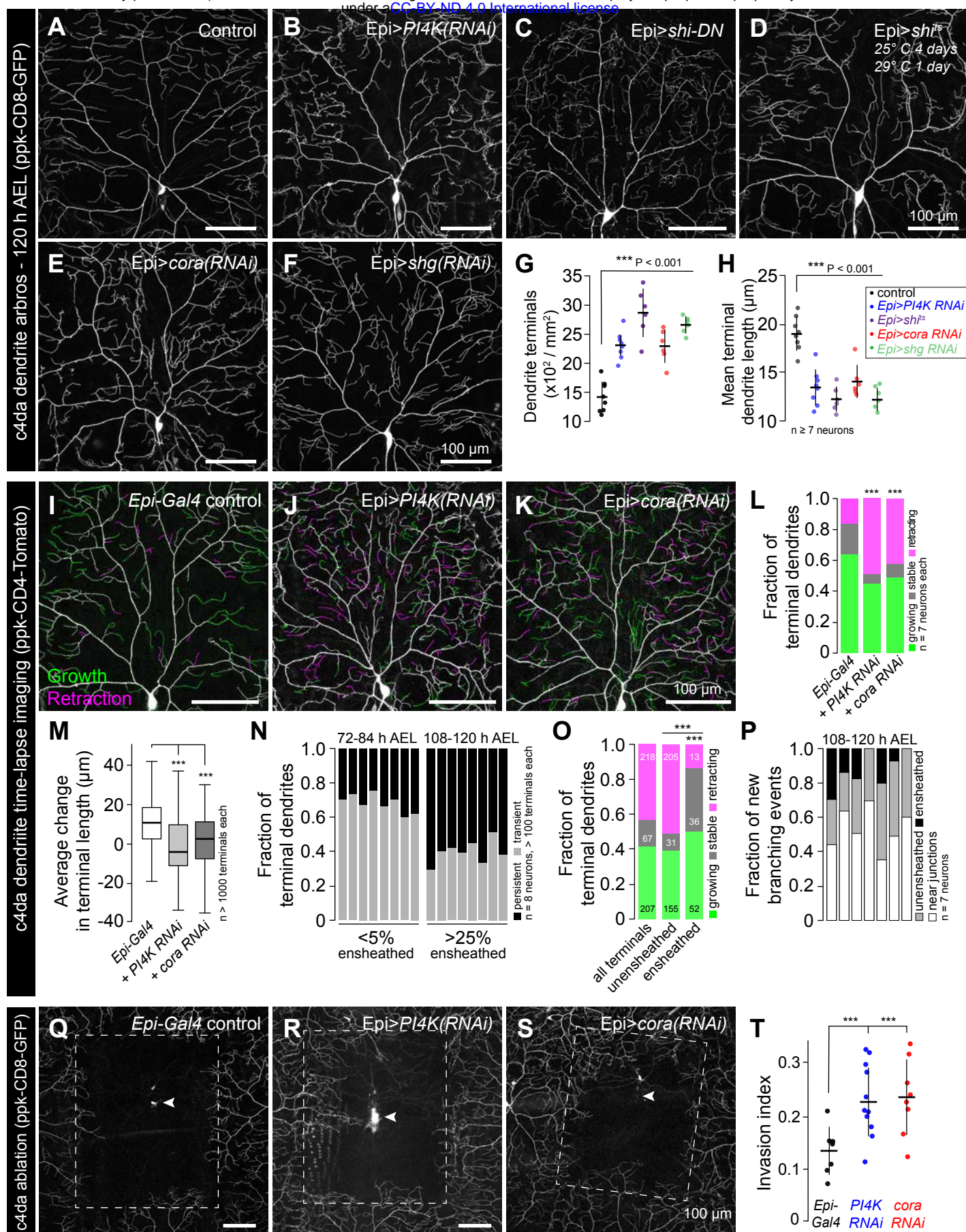


Figure 6. Epidermal sheaths regulate branching morphogenesis in nociceptive c4da neurons. Representative images of 120 h AEL c4da neurons from (A) control larvae and larvae expressing (B) *PI4K(RNAi)*, (C) dominant-negative *shibire* (*shi^{DN}*), (D) temperature-sensitive *shibire* (*shi^{ts}*), (legend continued on next page)

Figure 6. Epidermal sheaths regulate branching morphogenesis in nociceptive c4da neurons. Representative images of 120 h AEL c4da neurons from (A) control larvae and larvae expressing (B) *PI4K(RNAi)*, (C) dominant-negative *shibire* (*shi^{DN}*), (D) temperature-sensitive *shibire* (*shi^{ts}*), (E) epidermal *cora(RNAi)*, and (F) epidermal *shg(RNAi)* larvae are shown. Larvae were reared at 25° C with the exception of larvae in (D) which were reared at 25° C for 4 days and then shifted to the non-permissive temperature 29° C for 1 day prior to imaging. (G-H) Morphometric analysis of dendrites from c4da neurons of the indicated genotypes. Plots show mean and standard deviation for (G) the number of terminal branches and (H) terminal branch length. Data points, measurements from an individual neuron; ***P<0.001 relative to control; one way ANOVA with post-hoc Dunnett's test. (I-L) Time-lapse analysis of epidermal sheath control of terminal dendrite dynamics. C4da neurons were imaged over an 18 h time-lapse (96-114 h AEL) and growth (green) and retraction (magenta) were pseudocolored in a composite of the two time-points. Representative composite images are shown for c4da neurons from (I) Gal4-only control, (J) epidermal *PI4K(RNAi)* and (K) epidermal *cora(RNAi)* larvae. (L-P) Quantification of terminal dendrite dynamics. (L) The fraction of terminal dendrites that were growing, stable, or retracting over the time-lapse is shown. ***P<0.001 compared to controls, Chi-square analysis. (M) Epidermal ensheathment regulates the extent of terminal dendrite dynamics. Box plots depict mean values and 1st/3rd quartile, whiskers mark minimum/maximum values. ***P<0.001 compared to Epi-Gal4 control; one way ANOVA with post-hoc Dunnett's test. (N) Epidermal ensheathment regulates dendrite turnover. C4da neurons were imaged over a 12 h time-lapse (72-84 or 108-120 h AEL) and all terminal dendrites were scored as persistent (present at both time points) or transient. Each bar represents measurements from a single neuron. Terminal dendrites at the later time-point, when c4da neurons are extensively ensheathed, were significantly more likely to persist. (O) Quantification of terminal dynamics in ensheathed and unensheathed terminal dendrites from 108-120 h AEL. ***P<0.001, Chi-square analysis with post-hoc Bonferroni adjustment for multiple comparisons. Pairwise comparisons are indicated. (P) Distribution of branching events during 12 h time-lapse imaging. Each bar represents a single neuron. (Q-T) Epidermal ensheathment regulates dendrite structural plasticity. Class IV neurons in newly eclosed 2nd instar control (Q), epidermis *PI4k(RNAi)* (R), and epidermis *cora(RNAi)* (S) larvae were ablated with a focused laser beam and imaged 48hr post-ablation. Images depict dendrite growth of spared neurons into unoccupied territory following laser ablation and hatched boxes demarcate the territory occupied by the ablated neuron. (T) Scatter plot depicting mean and standard deviation for dendrite invasion of the indicated mutants. The number of samples analyzed for each treatment is indicated. ***P<0.001 relative to control; one way ANOVA with post-hoc Dunnett's test. .

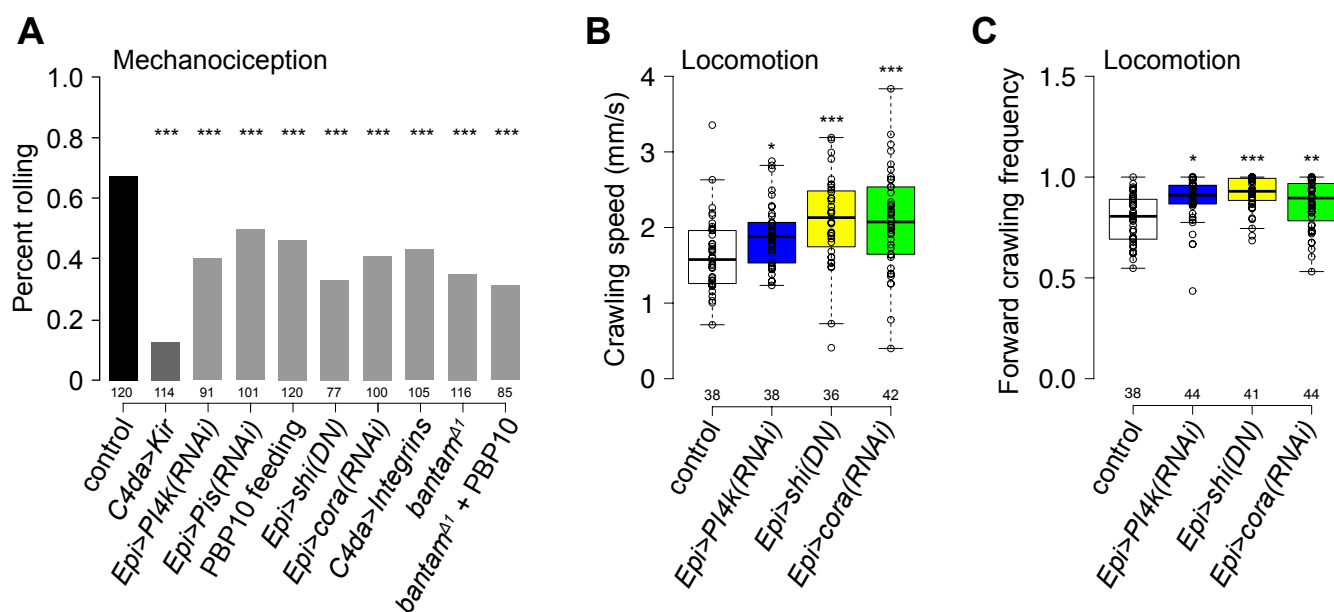


Figure 7. Epidermal dendrite ensheathment regulates nociceptive sensitivity. (A) Epidermal ensheathment regulates mechanonociception. Bars depict the proportion of larvae of the indicated genotype that exhibited a nocifensive rolling response to 70 mN von Frey fiber stimulation. *UAS-Kir2.1* expression in *c4da* neurons blocked nociceptive responses to 70 mN stimulus, demonstrating that the response is mediated by *c4da* neurons, and treatments that reduced epidermal ensheathment significantly reduced the frequency of nociceptive rolling responses. *** $P < 0.001$, compared to wt controls, Chi square test. (B-C) Epidermal ensheathment regulates the rate of larval locomotion. Box plots depict crawling speed (B) and the proportion of time larvae spent in forward-directed locomotion (C) for larvae of the indicated genotype. *** $P < 0.001$, * $P < 0.05$, Ns, not significant compared to wild type controls, Kruskal-Wallis rank sum test. The number of larvae tested is shown for each condition.